THE UNIVERSITY OF CALGARY

Development of A Real-Time Kinematic GPS System:

Design, Performance and Results

by

Hubiao Lan

A THESIS

SUBMITTED TO THE FACULTY OF GRADUATE STUDIES

IN PARTIAL FULFILLMENT OF THE REQUIREMENTS FOR THE

DEGREE OF MASTER OF SCIENCE

DEPARTMENT OF GEOMATICS ENGINEERING

CALGARY, ALBERTA

DECEMBER, 1996

0-612-20873-7

ABSTRACT

A real-time kinematic GPS system has been developed which achieves decimetre (with a floating ambiguity solution) and centimetre (with a fixed integer ambiguity solution) accuracies in real-time at a 1 Hz update rate. Based on a double difference floating ambiguity algorithm and a fast integer ambiguity search filter (FASF), the system resolves integer ambiguities if possible, or otherwise uses a floating ambiguity solution. The system integrates two L1 C/A code NovAtel GPSCard™ receivers (or two NovAtel OEM sensors), two portable computers and a pair of radio data transceivers. Carrier phase and pseudorange observations, as well as their corresponding corrections as defined by RTCM SC-104 types 18-21 are used for data communication. Performance of this system was evaluated by conducting both static and kinematic tests. Decimetre and centimetre accuracies were achieved for precision farming and kinematic surveying, respectively, in testing results.

ACKNOWLEDGMENTS

This research would have been impossible without the support and help of my supervisor Dr. M. E. Cannon. Her advice and guidance during my graduate study will be unforgettable in the rest of my life.

Special thanks go to Huangqi Sun in this department for his brotherly help both in China and Canada. The teaching and guidance of Dr. G. Lachapelle during my graduate studies are greatly appreciated. Special thanks also go to Jamie Henriksen for his help in the precision farming kinematic test, and his help to solve problems during the system development. Terry Labach at The U of C is thanked for his help in data communication during the development of the system.

Other students in the navigation group, namely Chuangya Tang, Shawn Weisenburger, Robert Harvey, and Weigen Qiu are thanked for their cooperation and fruitful discussions. They also provided a comfortable environment during my graduate studies.

Finally thanks to my wife, Weihua Shou for her love and understanding, and for her help during the kinematic test in Springbank.

The development of the RTK GPS system was partially supported by a contract between The U of C and the Naval Air Warfare Center, US Department of Navy.

TABLE OF CONTENTS

LIST OF TABLES

LIST OF FIGURES

NOTATIONS

i) Conventions

(a) Matrices are uppercase and bold

(b) Vectors are lower case and bold

(c) The operators are defined as:

Δ	single difference between receivers
∇	single difference between satellites
$\dot{\mathbf{a}}$	derivation with respect to time
(-)	Kalman prediction
(+)	Kalman update
$\mathbf{H}^T$	matrix transpose
$\mathbf{H}^{-1}$	matrix inverse
f()	is a function of
$\hat{\mathbf{x}}$	is an estimated value

ii) Acronyms

AS	Anti-Spoofing
AQ-Point™	An FM Radio Company in North America
C/A Code	Clear/Acquisition Code
DGPS	Differential GPS
ECEF	Earth-Centered-Earth-Fixed
FAA	Federal Aviation Administration
FARA	Fast Ambiguity Resolution Approach
FASF	Fast Ambiguity Search Filter
FDIR	Fault Detection, Identification and Recovery
GPS	Global Positioning System
ISA	Industrial Standard Architecture
LADGPS	Local Area Differential GPS
MDB	Minimal Detectable Biases
OEM	Original Equipment Manufacturer
OTF	On The Fly
P Code	Precise Code
PDOP	Position Dilution of Precision
PRN	Pseudo Random Noise
RTK	Real-Time Kinematic
RMS	Root Mean Square

RTCM	Radio Technical Commission for Marine Services
SA	Selective Availability
WAAS	Wide Area Augmentation System
WADGPS	Wide Area Differential GPS
WGS-84	World Geodetic System 1984

CHAPTER ONE

INTRODUCTION

1.1 Background and Objective

The Navstar Global Positioning System (GPS) is an advanced navigation satellite system for the determination of position, velocity and time. It can provide three-dimensional positioning on a global basis, independent of weather, 24 hours per day. GPS has been under development in the US since 1973 and originally functioned as a solely military system. The use of GPS is expanding rapidly in the civilian community due to decreasing in receiver costs [Lachapelle, 1995]. The current US government has stated that commercial users will continue to have access to GPS services without charge and that its current practice of selective availability (SA) will be terminated within 10 years [Space News, 1996].

Many GPS applications require accuracies from several metres to less than one metre, and they can be achieved by Differential GPS (DGPS) techniques [Abousalem, 1996]. However, sub-metre and even centimetre-level accuracy are required in many other applications, with some of these applications having real-time requirements: i.e. construction surveys, dredging, hydrographic and seismic surveys, and aircraft approach and landing [RTCM, 1994]. These applications all require that on-the-fly (OTF) ambiguity searching techniques operate in real-time. This is referred to as real-time kinematic (RTK) GPS operation. The concept of real-time kinematic GPS surveying was first described by Remondi [1985]. Since then, several methods have been developed to conduct kinematic surveying: i.e. semi-kinematic GPS [Cannon, 1989] and pseudo-kinematic GPS [Remondi, 1988]. Recent research has focused on OTF integer ambiguity resolution, and many methods have been developed for this purpose.

Although kinematic positioning algorithms were developed early in the late 1980's, no integrated real-time kinematic systems were operational until 1993. A fully integrated RTK system requires that GPS receivers are small, light-weight and need a low power supply. A moderate amount of computing power and data communications are also necessary. Additionally, the application of GPS to surveying and navigation was a gradual process, requiring time for testing and verification [Griffioen et al., 1993].

Several companies and organizations have developed RTK systems during the past few years. Trimble developed a high precision real-time system using its 4000SE/SSE GPS receivers [Griffioen et al., 1993]. This system outputs autonomous (single point) positions, double difference phase floating ambiguity positions and double difference phase fixed integer ambiguity positions (when the initialization is completed and both receivers maintain simultaneous lock on at least 4 common satellites). Ashtech developed a real-time GPS land surveying system based on its advanced Z-12 receivers and PNAV™ software [Gefsrud et al., 1995]. Making use of Z-Tracking™ technology, this system can measure C/A, P1, and P2 pseudoranges, in addition to carrier phase observations, whether or not anti-spoofing (AS) is operating. The ambiguity search algorithm fixes carrier phase integer ambiguities on-the-fly and generates centimetre level epoch-by-epoch position solutions. Both single frequency and dual frequency observations can be used to solve the ambiguities. If integer ambiguities cannot be fixed, the system will output floating ambiguity solutions. The US Army Topographic Engineering Center (TEC) and John E. Chance Associates, Inc. (JECA) developed a real-time OTF GPS positioning system for dredging [Frodge et al., 1995] which incorporates the OTF algorithm developed by Remondi [1991]. Centimetre level positioning accuracy was achieved with this system, using dual frequency Trimble 4000 SSE receivers, for baselines up to 25 km. NovAtel's RT20™ is a high performance floating ambiguity differential positioning package which promises to be as robust as a differential pseudorange system with position results approaching accuracies on the order of those achievable with a fixed ambiguity single frequency system [Ford and Neumann, 1994]. The basic algorithm uses a double difference floating ambiguity solution, based on carrier phase observations from NovAtel's C/A code GPS receiver (which uses Narrow Correlator technology [Fenton et al, 1991]). Test results for distances of 1-36 km demonstrate positioning accuracies of approximately 20 centimetres, after about 3 (10) minutes of static (kinematic) initialization. The newly released NovAtel's RT2 system is an expanded RT20 to take advantage of the dual frequency capability recently introduced by NovAtel [Neumann et al., 1996]. Test results show typical integer ambiguity resolution times of about 1 minute on short baseline, and typical horizontal accuracies of 1 to 2 cm. As for long baseline, the accuracy and integer ambiguity resolution time are gradually degraded. Several other groups have developed and tested RTK systems which are not described herein: McCall [1994]; Kelly [1992]; Walsh et al [1995]; Mathes and Gianniou [1994]; Dedes [1994].

The RTK GPS systems described above are commercial systems and their prices are generally high. In addition, the hardware and software are not easily adapted for various applications. The objective of this research is to develop an alternate short range RTK DGPS system witch encompasses the following features:

(1) lower cost achieved by using single frequency high performance C/A code GPS receivers;

(2) resolves integer ambiguies on-the-fly using a FASF algorithm;

(3) outputs both double difference floating ambiguity positions and double difference fixed integer ambiguity positions when appropriate;

(4) transmits and processes raw carrier phase, pseudorange, and Doppler observations, or alternatively carrier phase and pseudorange corrections;

(5) use RTCM SC-104 recommended standards;

(6) achieves centimetre level accuracies if possible, otherwise decimetre level accuracies;

(7) has high reliability.

1.2 Thesis Outline

Basic algorithms for the RTK GPS system are based on double difference floating and fixed integer ambiguity positioning solutions. Various GPS positioning techniques are introduced in Chapter Two, along with a description of the recent GPS positioning methodologies. The algorithm for the floating ambiguity solution is then derived, using Kalman filtering and least squares estimation, in Chapter Three. Additionally, the basic concepts of the Fast Ambiguity Search Filter (FASF) [Chen and Lachapelle, 1994], as applicable to this RTK GPS system, are also explained in Chapter Three.

Chapter Four describes the data transmission procedure for the developed RTK GPS system. Algorithms for generating the carrier phase and pseudorange corrections are then derived. Simple data transmission formats defined by the author during the development of the system are also introduced, and comparisons are made with RTCM types 18-19 formats in terms of transmission efficiency.

The hardware, software and system integration are described in Chapter Five. Quality control methods used to improve the reliability of the system are also described in Chapter Six. Chapter Seven contains a description of static and kinematic tests of the RTK GPS system, the results of which are also presented. Finally, conclusions and recommendations are presented in Chapter Eight.

CHAPTER TWO

GPS POSITIONING MODES

The basic GPS observations are pseudoranges, carrier phases and phase rates (Doppler). The basic observation equations for these observations are

$$P = \rho \qquad + c(d_t - d_T) + d_{ion} + d_{trop} + d_\rho + \varepsilon_P \,, \tag{2.1}$$

$$\Phi = \rho + \lambda N + c(d_t - d_T) - d_{ion} + d_{trop} + d_\rho + \varepsilon_\Phi \,, \tag{2.2}$$

$$\dot{\Phi} = \dot{\rho} \qquad + c(\dot{d}_t - \dot{d}_T) - \dot{d}_{ion} + \dot{d}_{trop} + \dot{d}_\rho + \varepsilon_{\dot{\Phi}} \,, \tag{2.3}$$

where P is the pseudorange observation (m),

Φ is the carrier phase observation (m),

$\dot{\Phi}$ is the Doppler observation (m s^{-1}),

ρ, $\dot{\rho}$ are the satellite-receiver geometric range and range rate, respectively (m, m s^{-1}),

λ is the carrier wavelength (m $cycle^{-1}$),

N is the carrier phase integer ambiguity (cycle),

c is the speed of light (m s^{-1}),

	d_t , $\dot{d}_t$	are the satellite clock error and error drift, respectively (m, m s^{-1}),
	d_T , $\dot{d}_T$	are the receiver clock error and error drift, respectively (m, m s^{-1}),
	d_{ion}, $\dot{d}_{ion}$	are the ionospheric delay and delay drift, respectively (m, m s^{-1}),
	d_{trop}, $\dot{d}_{trop}$	are the tropospheric delay and delay drift, respectively (m, m s^{-1}),
	d_ρ, $\dot{d}_\rho$	is the orbital error and error drift, respectively (m, m s^{-1}),
and	ε	is the measurement noise and multipath (m).

In equations (2.1) and (2.2), the satellite-receiver geometric range is calculated as $\rho = \left\| \mathbf{r}^S - \mathbf{r}^r \right\|$, where $\mathbf{r}^r$ is the unknown ECEF position vector of the receiver in WGS-84 and $\mathbf{r}^s$ is the ECEF position vector of the satellite in WGS-84, and $\dot{\mathbf{r}}^s$ is calculated from parameters included in the satellite ephemeris. The velocity of the receiver can be determined from equation (2.3), in which the range rate is computed as $\dot{\rho} = \left\| \dot{\mathbf{r}}^s - \dot{\mathbf{r}}^r \right\|$, where $\dot{\mathbf{r}}^r$ is the unknown velocity vector of the receiver and $\dot{\mathbf{r}}^s$ is the velocity vector of the satellite, which can also be calculated using the satellite ephemeris. The ionospheric delays in equations (2.1) and (2.2) are equal in magnitude, but opposite in sign. This property is often referred as code-carrier divergence [Hofmann-Wellenhof et al., 1994].

2.1 Point Positioning

If only one GPS receiver is used to generate position results, the position and velocity of the receiver can be solved by a least squares adjustment based on the observation equation given in equation (2.1) (see Figure 2.1). This positioning technique is referred to as point positioning. Unknown parameters in this method consist of the three coordinate components of the receiver position vector $\mathbf{r}^r$ and the receiver clock error d_T. At least four satellites are required at each epoch for a unique or overdetermined solution since there are four unknown parameters.

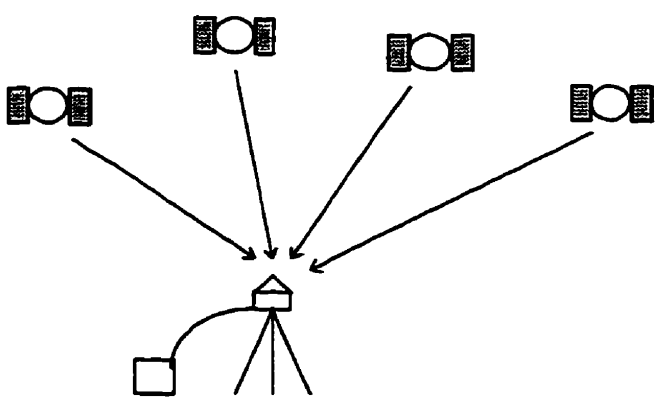

Figure 2.1: Point Positioning

For point positioning, all error sources are absorbed by the position except the receiver clock error, which is treated as an unknown and resolved [Hofmann-Wellenhof et al., 1994; Wells et al., 1986]. The unresolved error sources result in a less accurate positioning solution. These errors have been quantified [Lachapelle, 1995]: the normal satellite orbit error d_ρ is 5-10 m; the satellite clock error d_t is ~10 m; the SA effect on satellite orbit and clock is 5-80 m; the ionospheric delay is 2-50 m and the tropospheric delay is 2-30 m; and the pseudorange multipath and noise are 0.2-3 m and 0.1-3 m (1σ), respectively. With such error sources existing, the accuracy of pseudorange point positioning is over 100 m (2DRMS) when SA is on and broadcast ephemerides are used [Lachapelle, 1995]. To achieve higher accuracies, differential GPS (DGPS) techniques must be implemented.

2.2 DGPS Positioning

When two GPS receivers record observations from the same satellites simultaneously, the error sources can be reduced or eliminated through differential calculations. In this positioning method, one receiver is set at a reference station whose coordinates are known. The other receiver is designated as "the rover", whose coordinates are to be determined (see Figure 2.2).

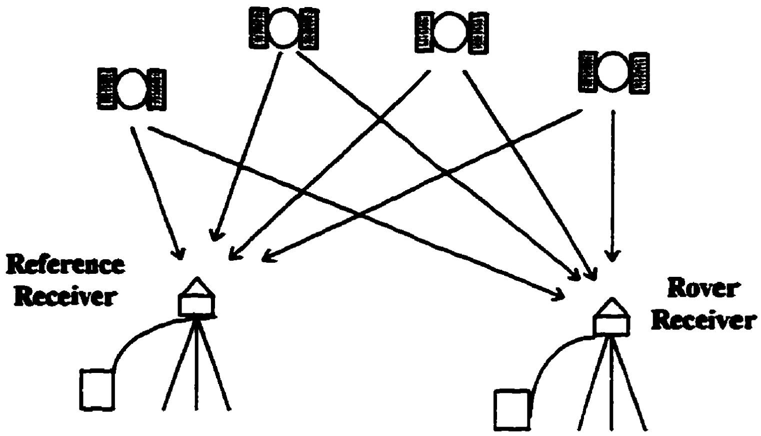

Figure 2.2: DGPS Positioning

Subtracting the observations at the reference station from those at the rover, the single difference observation equations are derived from equations (2.1), (2.2) and (2.3) as

$$\Delta P = \Delta\rho + c\Delta d_T + \Delta d_{ion} + \Delta d_{trop} + \Delta d_\rho + \varepsilon_{\Delta P} \,, \tag{2.4}$$

$$\Delta\Phi = \Delta\rho + \lambda\Delta N + c\Delta d_T - \Delta d_{ion} + \Delta d_{trop} + \Delta d_\rho + \varepsilon_{\Delta\Phi} \,, \tag{2.5}$$

$$\Delta\dot{\Phi} = \Delta\dot{\rho} + c\Delta\dot{d}_T - \Delta\dot{d}_{ion} + \Delta\dot{d}_{trop} + \Delta\dot{d}_\rho + \varepsilon_{\Delta\dot{\Phi}} \,, \tag{2.6}$$

where $\Delta = (\bullet)_{reference} - (\bullet)_{rover}$ is the single difference between receivers for a given satellite.

In the single difference equations, the satellite clock error, d_t, and its drift, $\dot{d}_t$, have been eliminated. Orbital error, as well as ionospheric and tropospheric delays, are reduced to small values (0.1 - 1 ppm for orbital error, 1 - 2 ppm for SA, 0.2 - 0.4 ppm and 0.3 - 3 ppm for ionospheric and tropospheric delays) if the distance between the reference station and the rover is less than 200 km [Abousalem, 1996]. Due to difficulties in solving for carrier phase integer ambiguities, pseudorange observations are often used to do single difference positioning. One to several metre DGPS positioning accuracy is feasible.

Instead of using raw pseudorange observations for positioning, carrier phase smoothed pseudoranges are used to achieve higher accuracy. The raw pseudorange is unambiguous but noisy, while the carrier phase is ambiguous but precise. Carrier phase integer ambiguities remain constant over time (unless cycle slips occur), and relative carrier phase differences between two epochs can therefore be measured accurately with a high degree of precision. The carrier phase smoothing method merges 'absolute' pseudorange capability and 'relative' carrier phase capability using a recursive filter [Lachapelle, 1995]. If carrier phase smoothing is performed, the accuracy of single difference DGPS positioning is 0.3-3 m horizontally and 0.5-4 m vertically over a 10 km reference-rover separation [Lachapelle, 1995].

By subtracting the single difference observations between a chosen (base) satellite and other satellites, double difference observation equations are derived as follows:

$$\nabla\Delta P = \nabla\Delta\rho \qquad + \nabla\Delta d_{ion} + \nabla\Delta d_{trop} + \nabla\Delta d_{\rho} + \varepsilon_{\nabla\Delta P}, \tag{2.7}$$

$$\nabla\Delta\Phi = \nabla\Delta\rho + \lambda\nabla\Delta N - \nabla\Delta d_{ion} + \nabla\Delta d_{trop} + \nabla\Delta d_{\rho} + \varepsilon_{\nabla\Delta\Phi}, \tag{2.8}$$

$$\nabla\Delta\dot{\Phi} = \nabla\Delta\dot{\rho} \qquad - \nabla\Delta\dot{d}_{ion} + \nabla\Delta\dot{d}_{trop} + \nabla\Delta\dot{d}_{\rho} + \varepsilon_{\nabla\Delta\dot{\Phi}}, \tag{2.9}$$

where $\nabla\Delta_i = \{(\bullet)_{reference} - (\bullet)_{rover}\}_i - \{(\bullet)_{reference} - (\bullet)_{rover}\}_{base}$,

i is the satellite number,

and base refers to the base satellite.

After the double difference calculations, satellite and receiver clock errors, and their corresponding drifts, are eliminated. Orbital errors, as well as ionospheric and tropospheric delays, are greatly reduced, as in the single difference case. These errors are spatially correlated [Hofmann-Wellenhof et al., 1994]. For short reference-rover separations (<10 km), the errors are generally small enough to be neglected. The only remaining errors are noise and multipath, such that equations (2.7) through (2.9) become

$$\nabla\Delta P \cong \nabla\Delta\rho \qquad + \varepsilon_{\nabla\Delta P}, \tag{2.10}$$

$$\nabla\Delta\Phi \cong \nabla\Delta\rho + \lambda\nabla\Delta N + \varepsilon_{\nabla\Delta\Phi}, \tag{2.11}$$

and $$\nabla\Delta\dot{\Phi} \cong \nabla\Delta\dot{\rho} \qquad + \varepsilon_{\nabla\Delta\dot{\Phi}}. \tag{2.12}$$

The noise and multipath of carrier phase observations are approximately 0.2 - 2 mm (0.1% to 1% of wavelength) and <0.25 λ (maximum) , respectively [Lachapelle, 1995]. In equations (2.8) and (2.11), the double difference carrier phase ambiguities are still integer numbers and are herein referred to as ambiguities. It is possible to solve for and fix the integer ambiguity term $\nabla\Delta N$ in equation (2.11) because the noise is less than one cycle.

For longer reference-rover separations (>10 km), total orbital errors (1 - 2 ppm), as well as ionospheric (0.2 - 0.4 ppm) and tropospheric (0.3 - 3 ppm) delays, decorrelate and cannot be eliminated. It is difficult to fix the correct integer ambiguities, since the wavelength of L1 is only 19.02 cm.

The highest accuracy GPS positioning can be achieved using the double difference carrier phase observation equation (2.8) or (2.11). If integer ambiguities in equation (2.11) are fixed for short reference-rover distances, centimetre level accuracies can be achieved. This is herein defined as the integer ambiguity solution, and will be discussed in Chapter Three. If instead the ambiguities are estimated as real numbers, decimetre accuracies are achieved. This is herein defined as the floating ambiguity solution, which will be discussed in Chapter Three.

2.3 Real-Time DGPS Positioning

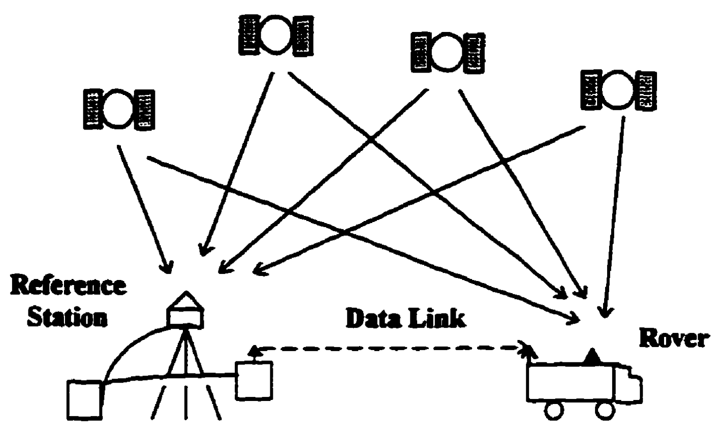

Figure 2.3: Real-Time DGPS Positioning

Many applications require a positioning accuracy of several metres for the rover in real-time. As described in the previous section, high accuracy is attainable through DGPS. In order to conduct DGPS positioning in real-time, data at the reference station is transmitted to the rover using a data link in order to form the differential observations (Figure 2.3).

The data link in Figure 2.3 may be a pair of radio transceivers [Dedes, 1994], a geo-stationary satellite link [Aparicio et al., 1994], a cellular phone [McCall, 1994] or FM radio [McLellan et al., 1994]. The minimum data transmission rate is 50 bits per second, and the typical time latency is a few to10 seconds (RTCM, 1994).

At the reference station, the combined effects (on a given pseudorange observation) of satellite clock error, satellite orbit error, ionospheric and tropospheric delays, and SA are computed from equation (2.1), using the known reference coordinates as input. These values, defined as pseudorange corrections, are transmitted to the rover via the data link. At the rover, the corrections are received and applied to the rover pseudorange observations, to form the single difference observations between the reference and rover receivers. Several metres positioning accuracy is achieved, depending on the reference-rover separation [Lachapelle, 1995].

Pseudorange corrections can also be generated using multiple reference stations in a local area (LADGPS) or a wide area (WADGPS) network [Robbins, 1994]. In this method, the pseudorange corrections are estimated from many reference stations separated by hundreds or thousands of kilometres and the positioning accuracy, reliability, and availability are improved [Abousalem, 1996]. Several WADGPS systems are in operation. Among these systems are ACCQPOINT™ (ACCQPOINT™ Communication Corporation, EAGLE™ (Differential Corrections Inc.), OMNISTAR™ (Fugro Group of Companies), FAA's Wide Area Augmentation System (WAAS), SkyFix™ (Racal Surveys Ltd.) and STARFIX® system (John E. Chance & Associates) [Abousalem, 1996].

2.4 RTK GPS Positioning

To achieve higher positioning accuracies (decimetre or centimetre level) in real-time, the double differencing technique should be implemented using carrier phase data. This requires that the raw pseudorange and carrier phase observations, or their corrections, are transmitted from the reference station to the rover using a 0.5 - 2 seconds update rate [RTCM, 1994]. This is defined as real-time kinematic (RTK) GPS positioning.

Since spatial decorrelation degrades the accuracy of double difference observations, the reference-rover separation should be limited to tens of kilometres (depending on whether single or dual frequency receivers are used). The integer ambiguities can be fixed "on-the-fly" (OTF) or solved for as real numbers (float solution). Once the integer ambiguities have been fixed, centimetre level accuracies can be achieved. Alternatively, decimetre level accuracies are typically achieved using the floating ambiguity solution. These two types of real-time positioning solutions are discussed in Chapter Three.

CHAPTER THREE

FLOATING AND FIXED INTEGER AMBIGUITY SOLUTIONS

RTK GPS positioning requires that double difference carrier phase ambiguities are determined in real-time. In this chapter, equations for the floating ambiguity solution are given, based on the standard Kalman filter equations. An equivalent least squares approach is also derived, and used to develop the RTK GPS system specific to this thesis research. The FASF ambiguity searching algorithm is also introduced, in addition to the fixed integer ambiguity solution.

3.1 Floating Ambiguity Solution

In kinematic GPS positioning, the rover dynamics are often described by a constant velocity model [Cannon, 1991]. If the carrier phase ambiguities are treated as real numbers, the state equation of the rover is as follows [Gelb, 1974]:

$$\dot{\mathbf{x}} = \mathbf{F}\,\mathbf{x} + \mathbf{w}\,, \tag{3.1}$$

where $\mathbf{x}$ represents $\left\{ \delta x,\ \delta y,\ \delta z,\ \delta v_x,\ \delta v_y,\ \delta v_z,\ \delta\Delta\nabla N_1,\ \delta\Delta\nabla N_2, \cdots,\ \delta\Delta\nabla N_{n-1} \right\}^T$, the state vector of dimension $(m \times 1)$, where m is the number of parameters,

$\{\delta x, \delta y, \delta z\}^T$ are corrections to the position vector of the rover receiver in WGS-84,

$\{\delta v_x, \delta v_y, \delta v_z\}^T$ are corrections to the velocity vector of the rover receiver in WGS-84,

$\{\delta\Delta\nabla N_1, \delta\Delta\nabla N_2, \cdots, \delta\Delta\nabla N_{n-1}\}^T$ are corrections to the unknown carrier phase double difference ambiguities, and n is the number of satellites,

$\mathbf{w} = \left[w_x, w_y, w_z, 0, 0, \cdots, 0\right]^T$ is the system noise vector $(m \times 1)$,

and F is the dynamics matrix $(m \times m)$ with the form [Cannon, 1991]

$$\mathbf{F} = \begin{pmatrix} 0\,0\,0\,1\,0\,0\,0\,0 \cdots 0 \\ 0\,0\,0\,0\,1\,0\,0\,0 \cdots 0 \\ 0\,0\,0\,0\,0\,1\,0\,0 \cdots 0 \\ 0\,0\,0\,0\,0\,0\,0\,0 \cdots 0 \\ 0\,0\,0\,0\,0\,0\,0\,0 \cdots 0 \\ 0\,0\,0\,0\,0\,0\,0\,0 \cdots 0 \\ 0\,0\,0\,0\,0\,0\,0\,0 \cdots 0 \\ 0\,0\,0\,0\,0\,0\,0\,0 \cdots 0 \\ \cdots\cdots\cdots\cdots\ 0 \\ \cdots\cdots\cdots\cdots\ 0 \\ \cdots\cdots\cdots\cdots\ 0 \\ 0\,0\,0\,0\,0\,0\,0\,0 \cdots 0 \end{pmatrix}.$$

This model is based on the assumption that acceleration during the period Δt (1 second in this system) is zero. For a high dynamics environment and low data rate, this model is not complete. Effects of the modelling error can be absorbed by increasing the process noise.

A better approach is to model the system dynamics as a first-order Gauss-Markov process:

$$\dot{\mathbf{x}} = -\beta \mathbf{x} + \mathbf{w} , \tag{3.2}$$

where $1/\beta$ is referred to as correlation time [Gelb, 1974].

The rover position is determined using the Kalman filter equations where the double difference observation equations (2.7) to (2.9) are used to calculate updates. Traditional Kalman filter equations are reviewed in Appendix. In the following sections, an equivalent least squares approach is introduced and incorporated into the development of the RTK system in this research.

The Kalman filter equations can also be derived from a least squares approach using a simple parametric model [Krakiwsky, 1990]. The advantage of this approach is that Kalman filtering can be implemented by a simple sequential least square approach, and many available formulae for least squares estimation can then be used in kinematic processing. The least squares approach detailed below has been used in developing the RTK GPS system for this thesis research.

Suppose that it is necessary to estimate the state vector $\mathbf{x}_{k+1}$ at epoch k+1 in terms of the observation vector $\mathbf{l}_{k+1}$, its covariance matrix $\mathbf{C}^{\varepsilon}$ and the estimated state vector $\hat{\mathbf{x}}_k$ at epoch k. Also suppose that $\mathbf{v}_{k+1}$ is the correction (residual) of $\mathbf{l}_{k+1}$. The relationship between $\mathbf{l}_{k+1}$ and $\mathbf{x}_{k+1}$ is modelled by

$$\mathbf{l}_{k+1} + \mathbf{v}_{k+1} = f(\mathbf{x}_{k+1}), \tag{3.3}$$

where $\mathbf{v}_{k+1}$ is assumed to have zero-mean Gaussian distribution $\mathbf{v}_{k+1} \sim N(0, \mathbf{C}^{\varepsilon})$.

The relationship between $\mathbf{x}_{k+1}$ and $\mathbf{x}_k$ is modelled by

$$\mathbf{x}_{k+1} = g(\mathbf{x}_k, t_{k+1}, t_k) + \varepsilon_k, \tag{3.4}$$

where ε_k is the uncertainty of the dynamic model assumed with zero-mean Gaussian distribution $\varepsilon_k \sim N(0, \mathbf{C}_k^w)$, and its variance-covariance matrix is $\mathbf{C}_k^w$ as described in Appendix.

Assuming $\hat{\mathbf{x}}_k$ is the state vector estimation computed from all information up to epoch k, the predicted value of the state vector can be computed from equation (3.4) as

$$\mathbf{x}_{k+1}(-) = \mathbf{g}(\hat{\mathbf{x}}_k,\, t_{k+1},\, t_k) + \varepsilon_k\,. \tag{3.5}$$

Here the symbol $\wedge$ means least squares estimate, (-) denotes predicted quantities, (+) denotes updated quantities,

Linearizing equation (3.5) using a Taylor's series, the linearized model becomes

$$\mathbf{x}_{k+1}(-) = \Phi_{k+1,k}(\hat{\mathbf{x}}_k - \mathbf{x}_{k0}) + \mathbf{g}(\mathbf{x}_{k0},\, t_{k+1},\, t_k) + \varepsilon_k\,, \tag{3.6}$$

where $\Phi_{k+1,k} = \left.\dfrac{\partial \mathbf{g}}{\partial \mathbf{x}}\right|_{\mathbf{x}_{k0}}$,

and $\mathbf{x}_{k0}$ is the point of expansion.

By using the law of error propagation, the covariance matrix of the predicted state vector can be computed as

$$\mathbf{C}_{x_{k+1}(-)} = \Phi_{k+1,k}\mathbf{C}_{\hat{x}_k}\Phi^T_{k+1,k} + \mathbf{C}^w_k\,. \tag{3.7}$$

The observation equation (3.3) can be linearized using $\mathbf{x}_{k+1}(-)$ as

$$\mathbf{v}_{k+1} = \mathbf{H}_{k+1}\delta_{k+1} + \mathbf{w}_{k+1}, \tag{3.8}$$

where $\mathbf{H}_{k+1} = \frac{\partial \mathbf{f}}{\partial \mathbf{x}}\Big|\mathbf{x}_{k+1}(-)$ is the design matrix,

δ_{k+1} is the correction to the predicted value $\mathbf{x}_{k+1}(-)$,

and $\mathbf{w}_{k+1} = f(\mathbf{x}_{k+1}(-)) - \mathbf{l}_{k+1}$.

The predicted state vector can also be treated as an observation. The observation equation corresponding to the predicted state vector is

$$\mathbf{v}_{k+1}(-) = \delta_{k+1} . \tag{3.9}$$

Combining equation (3.8) and (3.9) into one, we get a combined observation equation

$$\mathbf{v} = \mathbf{H}\delta_{k+1} + \mathbf{w}, \tag{3.10}$$

where $\mathbf{v} = \begin{pmatrix} \mathbf{v}_{k+1}(-) \\ \mathbf{v}_{k+1} \end{pmatrix}$,

$\mathbf{H} = \begin{pmatrix} \mathbf{I} \\ \mathbf{H}_{k+1} \end{pmatrix}$,

$$\mathbf{w} = \begin{pmatrix} \mathbf{0} \\ \mathbf{w}_{k+1} \end{pmatrix}, \tag{3.11}$$

with a variance-covariance matrix

$$\mathbf{C} = \begin{pmatrix} \mathbf{C}_{x_{k+1}(-)} & \mathbf{0} \\ \mathbf{0} & \mathbf{C}^{\varepsilon} \end{pmatrix}. \tag{3.12}$$

The estimated state vector and its covariance matrix can be derived using a least square parametric adjustment model as follows:

$$\hat{\delta}_{k+1} = -\left[\mathbf{H}^T\mathbf{C}^{-1}\mathbf{H}\right]^{-1}\mathbf{H}^T\mathbf{C}^{-1}\mathbf{w},$$

$$\begin{aligned} \hat{\mathbf{x}}_{k+1} &= \mathbf{x}_{k+1}(-) + \hat{\delta}_{k+1} \\ &= \mathbf{x}_{k+1}(-) - \left[\mathbf{H}^T\mathbf{C}^{-1}\mathbf{H}\right]^{-1}\mathbf{H}^T\mathbf{C}^{-1}\mathbf{w}, \end{aligned}$$

and $$\mathbf{C}_{\hat{x}_{k+1}} = \left[\mathbf{H}^T\mathbf{C}^{-1}\mathbf{H}\right]^{-1}. \tag{3.13}$$

By substituting equations (3.11) and (3.12) into equation (3.13), the following equations can be derived:

$$\hat{\mathbf{x}}_{k+1} = \mathbf{x}_{k+1}(-) - \left[\mathbf{C}^{-1}_{x_{k+1}(-)} + \mathbf{H}_{k+1}{}^T\mathbf{C}^{\varepsilon^{-1}}\mathbf{H}_{k+1}\right]^{-1}\mathbf{H}^T_{k+1}\mathbf{C}^{\varepsilon^{-1}}\mathbf{w}_{k+1}$$

$$= \mathbf{x}_{k+1}(-) - \mathbf{K}\mathbf{w}_{k+1}, \tag{3.14}$$

$$\begin{aligned}
\mathbf{C}_{\hat{\mathbf{x}}_{k+1}} &= \left[\mathbf{C}^{-1}_{\mathbf{x}_{k+1}(-)} + \mathbf{H}^{T}_{k+1}\mathbf{C}^{\varepsilon^{-1}}\mathbf{H}_{k+1}\right]^{-1} \\
&= \mathbf{C}_{\mathbf{x}_{k+1}(-)} - \mathbf{C}_{\mathbf{x}_{k+1}(-)}\mathbf{H}^{T}_{k+1}\left[\mathbf{C}^{\varepsilon} + \mathbf{H}^{T}_{k+1}\mathbf{C}_{\mathbf{x}_{k+1}(-)}\mathbf{H}_{k+1}\right]^{-1}\mathbf{H}_{k+1}\mathbf{C}_{\mathbf{x}_{k+1}(-)} \\
&= \left[\mathbf{I} - \mathbf{K}\mathbf{H}_{k+1}\right]\mathbf{C}_{\mathbf{x}_{k+1}}(-),
\end{aligned} \tag{3.15}$$

and

$$\begin{aligned}
\mathbf{K} &= \mathbf{C}_{\mathbf{x}_{k+1}(-)}\mathbf{H}^{T}_{k+1}\left[\mathbf{C}^{\varepsilon} + \mathbf{H}^{T}_{k+1}\mathbf{C}_{\mathbf{x}_{k+1}(-)}\mathbf{H}_{k+1}\right]^{-1}\mathbf{H}_{k+1}\mathbf{C}_{\mathbf{x}_{k+1}(-)} \\
&= \left[\mathbf{C}^{-1}_{\mathbf{x}_{k+1}(-)} + \mathbf{H}_{k+1}{}^{T}\mathbf{C}^{\varepsilon^{-1}}\mathbf{H}_{k+1}\right]^{-1}\mathbf{H}^{T}_{k+1}\mathbf{C}^{\varepsilon^{-1}}.
\end{aligned} \tag{3.16}$$

Comparing equations (A.5)-(A.8) with equations (3.14)-(3.16), it can be seen that the equations are the same but with different notations.

3.2 Fixed Integer Ambiguity Solution

Using the carrier phase observation equation (2.8), with the double difference integer ambiguities fixed correctly, the position of the rover can be solved using a simple parametric least squares model. The highest accuracy (centimetre level) is achieved using the carrier phase observations of at least four satellites. The observation equation at a given epoch is

$$\mathbf{l} + \mathbf{v} = \mathbf{H}\mathbf{x},$$

and $$\mathbf{v} = \mathbf{H}\delta + \mathbf{w}, \tag{3.17}$$

where $\mathbf{l}$ is the double difference carrier phase observations,

$\mathbf{v}$ is the residual of $\mathbf{l}$ with zero-mean Gaussian distribution and a variance-covariance matrix $\mathbf{C}^{\varepsilon}$, $\mathbf{v} \sim N(0, \mathbf{C}^{\varepsilon})$,

$\mathbf{H}$ is the double difference carrier phase design matrix,

$\mathbf{x}$ is the position vector,

$\delta = \mathbf{x} - \mathbf{x}_0$ is the correction vector of $\mathbf{x}$ with respect to the approximate position vector $\mathbf{x}_0$,

and $\mathbf{w} = \mathbf{H}\mathbf{x}_0 - \mathbf{l}$.

Solving the observation equation (3.17) using the least squares method, the least squares estimation of the position vector is derived as

$$\hat{\mathbf{x}} = \mathbf{x}_0 + \left[\mathbf{H}^T \mathbf{C}^{\varepsilon^{-1}} \mathbf{H}\right]^{-1} \mathbf{H}^T \mathbf{C}^{\varepsilon^{-1}} \mathbf{w}. \tag{3.18}$$

The variance-covariance matrix of $\hat{\mathbf{x}}$ is

$$\mathbf{C}_{\hat{x}} = \left[\mathbf{H}^T \mathbf{C}^{\varepsilon^{-1}} \mathbf{H}\right]^{-1} . \tag{3.19}$$

It is noted that the double difference observations are correlated, so the variance-covariance matrix $\mathbf{C}^{\varepsilon}$ takes the following form:

$$\mathbf{C}^{\varepsilon} = 2\,\sigma^2 \begin{bmatrix} 2 & 1 & \dots & 1 \\ 1 & 2 & \dots & 1 \\ \dots & \dots & \dots & \dots \\ 1 & 1 & \dots & 2 \end{bmatrix} . \tag{3.20}$$

where σ^2 is the *a-priori* variance of carrier phase observations. The standard deviation σ is adjusted according to the reference-rover distance (1 ppm was used in this system).

The most important factor in the fixed integer ambiguity solution is an integer ambiguity search which determines the correct integer ambiguity combination. There are many papers on OTF integer ambiguity resolution, using methods such as least squares searching [Hatch, 1991], the ambiguity function method [Mader, 1990], the fast ambiguity resolution approach (FARA) [Frei and Beutler, 1990], and the fast ambiguity search filter (FASF) [Chen and Lachapelle, 1994]. FASF is used in developing the RTK GPS system for this thesis research. The FASF algorithm is described below. See Chen and Lachapelle [1994], and Lu [1994] for further details.

In the FASF, the ambiguity search range is determined recursively for each satellite ambiguity. The effect of an assumed integer ambiguity on the other satellite ambiguities is then fully accounted for when determining the search range of other ambiguities. Furthermore, all observations, from the initial epoch to the current epoch, are accounted for through a floating ambiguity solution.

FASF is based on the floating ambiguity solution in which the estimates of rover position, velocity, and the ambiguity values ($\hat{\mathbf{x}} = \left\{ \hat{x},\ \hat{y},\ \hat{z},\ \hat{v}_x,\ \hat{v}_y,\ \hat{v}_z,\ \Delta\nabla\hat{N}_1,\ \Delta\nabla\hat{N}_2,\ \cdots,\ \Delta\nabla\hat{N}_{n-1} \right\}^T$), in addition to their variance-covariance matrix ($\mathbf{C}_{\hat{x}}$) and the quadratic form of the residuals ($\Omega = \mathbf{v}^T \mathbf{C}^{\varepsilon^{-1}} \mathbf{v}$), are obtained. The search range for the integer ambiguity $\nabla\Delta N_{n-1}$ is defined as

$$\nabla\Delta\hat{N}_{n-1} - k\sigma_{\nabla\Delta N_{n-1}} \leq \nabla\Delta N_{n-1} \leq \nabla\Delta\hat{N}_{n-1} + k\sigma_{\nabla\Delta N_{n-1}}\ , \qquad (3.21)$$

where $\nabla\Delta\hat{N}_{n-1}$ and $\sigma_{\nabla\Delta N_{n-1}}$ are the estimates of $\nabla\Delta N_{n-1}$ and its standard deviation, respectively, as given by the floating ambiguity solution. k is a constant scale factor, which is assigned a value between 3 and 10, depending on the error behavior in the observations [Lu, 1995] (here 5 is selected in this research). Setting $\nabla\Delta N_{n-1}$ to a given integer value $\nabla\Delta\overline{N}_{n-1}$, inside the search range defined by (3.21), is equivalent to adding a constraint to the floating ambiguity solution [Lu, 1995]. By using the least squares formulae with constraints, the updated solution in which $\nabla\Delta N_{n-1}$ is set to an integer value $\nabla\Delta\overline{N}_{n-1}$, is derived as

$$\hat{x}(n-1) = \hat{x} - C_{n+5} \cdot (\nabla\Delta\hat{N}_{n-1} - \nabla\Delta\overline{N}_{n-1}) / (C_{\hat{x}})_{n+5,n+5} \,, \tag{3.22}$$

$$C_{\hat{x}}(n-1) = C_{\hat{x}} - C_{n+5} \cdot C_{n+5}^{T} / (C_{\hat{x}})_{n+5,n+5} \,, \tag{3.23}$$

$$\Omega(n-1) = \Omega + (\nabla\Delta\hat{N}_{n-1} - \nabla\Delta\overline{N}_{n-1})^2 / (C_{\hat{x}})_{n+5,n+5} \,, \tag{3.24}$$

here (n-1) refers to the new solution with assumed integer ambiguity $\nabla\Delta\overline{N}_{n-1}$, while $C_{n+5} = [(C_{\hat{x}})_{1,n+5} \; (C_{\hat{x}})_{2,n+5} \cdots (C_{\hat{x}})_{n+5,n+5}]$ is the last column related to $\nabla\Delta N_{n-1}$ in matrix $C_{\hat{x}}$. $(C_{\hat{x}})_{n+5,n+5}$ is the diagonal element relating to $\nabla\Delta N_{n-1}$ in $C_{\hat{x}}$.

It can be observed from equation (3.23) that the diagonal elements in the variance-covariance matrix $C_{\hat{x}}(n-1)$ are always smaller than those in the original variance-covariance matrix $C_{\hat{x}}$: this implies that ambiguity search intervals for the remaining ambiguities will be reduced by fixing $\nabla\Delta N_{n-1}$ to an integer number $\nabla\Delta\overline{N}_{n-1}$. Additionally, the residual quadratic form $\Omega(n-1)$ can easily be computed using equation (3.24), and it is always larger than the residual quadratic form of the floating ambiguity solution. For this reason, an early exit from the searching algorithm is possible [Lu, 1995].

A Chi-square local test is used to determine whether the given integer ambiguity $\nabla\Delta\overline{N}_{n-1}$ is retained as part of the solution or rejected. Under a certain level of significance α (α = 0.05 is used in this research) and corresponding degrees of freedom f, the decision to reject or retain $\nabla\Delta\overline{N}_{n-1}$ is determined according to the following criteria:

$$\Omega(n) > \chi^2(f,\ 1-\alpha),\ \text{rejected,}$$

$$\text{or} \qquad \Omega(n) \leq \chi^2(f,\ 1-\alpha),\ \text{retained.} \tag{3.25}$$

If $\nabla\Delta\overline{N}_{n-1}$ passes the test, this integer value is combined directly with possible ambiguities for the second ambiguity term $\nabla\Delta N_{n-2}$, whose search range is bounded by the second last diagonal element in $C_{\hat{x}}(n-1)$, assuming the ambiguity $\nabla\Delta N_{n-1}$ is fixed. With the substitution of $(\hat{x}(n-1), C_{\hat{x}}(n-1), \Omega(n-1))$ in place of $(\hat{x}, C_{\hat{x}}, \Omega)$, the whole algorithm from equation (3.22) to (3.25) is then repeated, and $\nabla\Delta N_{n-2}$ is fixed to an integer number within its search range.

The recursive updating and testing process continues until all the possible ambiguities for all satellites are searched. If only one combination of all the ambiguities remains and passes the test, those integer ambiguities are considered to be correct. If more than one integer ambiguity combination is available, the ratio test (the smallest residual quadratic form Ω_{min1} compared to the second smallest residual quadratic form Ω_{min2}) is performed.

If the ratio $\Omega_{min2}/\Omega_{min1}$ is bigger than a predefined threshold (3.0 is used in this research), the ambiguity combination associated with Ω_{min1} is selected. In the case that integer ambiguities cannot be fixed, the whole ambiguity search process will start again at the next epoch, using the floating ambiguity solution from the next epoch.

Both land and airborne test results demonstrate that FASF reduces both the computation and observation times required for ambiguity resolution OTF, as compared to the least-squares search method (see Chen and Lachapelle [1994] for details).

CHAPTER FOUR

DATA TRANSMISSION FROM THE REFERENCE STATION TO THE ROVER

4.1 Data Transmission Procedure

For RTK applications, the required update rate is much higher than that for conventional DGPS, since double difference carrier phase observations are formed at the rover and a centimetre level accuracy is desired. Data must be updated every 0.5~2 seconds (1 second in this system), rather than every ~10 seconds for conventional DGPS. As a consequence, the data links are more likely to utilize UHF/VHF radio transceivers with transmission rates of 1200~9600 baud [RTCM, 1994]. Figure 4.1 shows the general data transmission process between a pair of radio transceivers [Proakis, 1989] in this RTK GPS system.

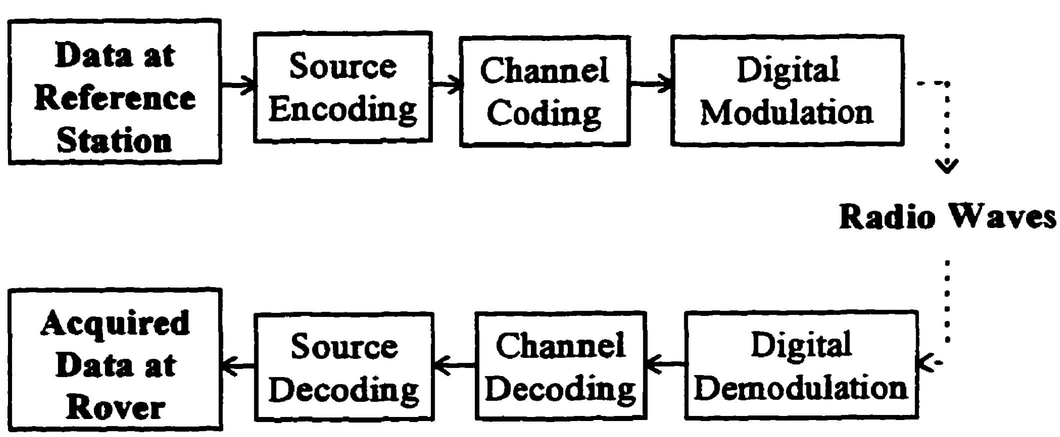

Figure 4.1: Data Transmission Process

Data at the reference station are in digital format and ready for transmission. After source encoding and channel coding, the digital symbols are transformed into radio waves by a digital modulator. At the rover location, the radio waves are received by a radio transceiver and transformed into digital format by the digital demodulator. After channel decoding and source decoding, data from the reference station are acquired by the rover.

Most of the transmission process shown in Figure 4.1 is performed automatically by the radio transceivers. However, encoding the data into predefined formats at the reference station (source encoding) and decoding the acquired data at the rover (source decoding) are required. For the RTK GPS system in this research, the data transmitted is either carrier phase and pseudorange observations or their corrections.

4.2 Carrier Phase and Pseudorange Corrections Versus Uncorrected Observations

Uncorrected carrier phase and pseudorange observations at the reference station can be transmitted and used to form double difference observations at the rover (see equations 2.7-2.9). Alternatively, another option is to transmit both carrier phase and pseudorange corrections (i.e. DGPS).

There are several advantages in transmitting carrier phase and pseudorange corrections, as opposed to the uncorrected observations. Since the magnitude of pseudorange and carrier phase correction values is smaller than that of the uncorrected pseudorange and carrier phase observations, fewer bits are required for the transmission of corrections than that for the transmission of uncorrected observations (see the U of C format in Section 4.3.2). Furthermore, the number of computations required at the rover is reduced when corrections, rather than uncorrected observations, are used [Blomenhofer and Hein, 1994].

4.2.1 Carrier Phase and Pseudorange Corrections

It is more complicated to generate carrier phase corrections than pseudorange corrections at the reference station, since it is necessary to consider the carrier phase integer ambiguities. To determine the carrier phase corrections, each phase observation is first assigned an approximate integer ambiguity. Those ambiguities are set such that the carrier phase observations best agree with the code observations for the first epoch (t_0) at which the satellite is acquired by the receiver: i.e.

$$N_R^S = \mathrm{INT}(P_R^S(t_0)/\lambda - \varphi_R^S(t_0)), \tag{4.1}$$

where N_R^S is the approximate integer ambiguity for satellite S at receiver R (cycles),

INT is the closest integer operator

$P_R^S(t_0)$ is the code measurement at time t_0 (metres),

λ is the signal wavelength (metres/cycle),

and $\varphi_R^S(t_0)$ is the carrier phase observation at time t_0 (cycles).

The measured carrier phase $\varphi_R^S(t_0)$ is modified by N_R^S to give the modified carrier phase observation

$$\varphi R_R^S = \varphi_R^S(t_0) + N_R^S \quad . \tag{4.2}$$

Secondly, an algorithm is implemented to remove the effect of the reference clock bias from the phase correction. This is described in the following steps.

At the first epoch t_0 for each satellite, the difference D^S (between the modified carrier phase measurement and the estimated satellite-receiver range using the known reference coordinates) is computed in cycles:

$$D^S = \rho_R^S(t_0)/\lambda - \varphi R_R^S(t_0), \tag{4.3}$$

where $\rho_R^S(t_0)$ is the computed satellite-receiver range for satellite S at time t_0 in metres.

The mean value of these differences for all available satellites is calculated:

$$\delta t_R(t_0) = \frac{\sum_{s=1}^{n} (\rho_R^S(t_0)/\lambda - \varphi R_R^S(t_0))}{n}, \tag{4.4}$$

where n is the number of satellites available at the first epoch.

The value $\delta t_R(t_0)$ is treated as the clock bias, which can be removed from the difference D^S for each satellite forming a phase correction:

$$\varphi C_R^S(t_0) = \rho_R^S(t_0)/\lambda - \varphi R_R^S(t_0) - \delta t_R(t_0). \tag{4.5}$$

At the following measurement epochs ($t > t_0$), differences between modified carrier phase observations and the estimated satellite-receiver ranges are formed again for each available satellite. Change in D^S for each satellite, from one epoch to the next, is given by

$$\Delta D^S = (\rho_R^S(t) - \rho_R^S(t-1))/\lambda - (\varphi R_R^S(t) - \varphi R_R^S(t-1)), \tag{4.6}$$

The mean value of ΔD^S is calculated using ΔD^S values from all available satellites, and is attributed to a change in the clock bias. The clock bias (in cycles) at epoch t-1 is then updated for epoch t, using

$$\delta t_R(t) = \delta t_R(t-1) + \frac{\sum_{s=1}^{n} \Delta D^S}{n} . \tag{4.7}$$

The phase correction (in cycles) for satellite S at epoch t can then be computed using the equation

$$\varphi C_R^S(t) = \rho_R^S(t) / \lambda - \varphi R_R^S(t) - \delta t_R(t) . \tag{4.8}$$

It is advantageous to consider changes of D^S from epoch to epoch (ΔD^S), such that variations in the satellite configuration do not cause discontinuities in estimates of the clock bias.

Figures 4.2 and 4.3 show sample carrier phase corrections as a function of GPS time. The data was collected on October 8, 1994, during which time SA was operating.

PRN 12 is a BLOCK I satellite and is not directly affected by SA. Its phase corrections, however, reflect the mean effect of SA on the computed receiver clock bias. Phase corrections for Block II satellite, PRN 23, are directly affected by SA, such that the variations in PRN 23 phase corrections are larger than that those for PRN 12.

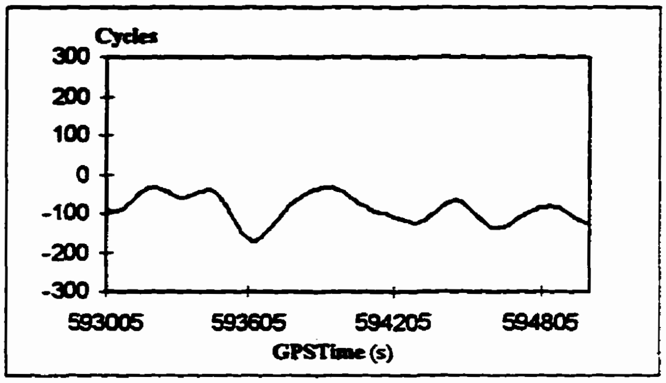

Figure 4.2: Carrier Phase Corrections for PRN 12, October 8, 1994

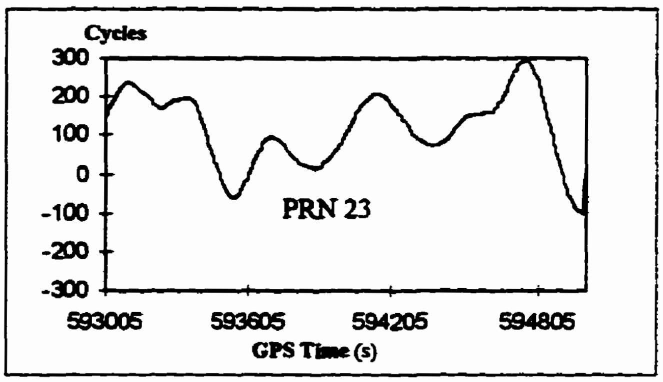

Figure 4.3: Carrier Phase Corrections for PRN 23, October 8, 1994

The algorithm used to generate pseudorange corrections at the reference station is identical to the one described above except that the ambiguities are not considered (i.e. equations (4.1) and (4.2) are not required). The correction rate can be generated by differencing two pseudorange observations from consecutive epochs or, alternatively, using the Doppler observations.

4.2.2 Use of Corrections at the Rover

Carrier phase and pseudorange observations at the rover are corrected using the corrections transmitted from the reference station, i.e.

$$\breve{\varphi}_U^S = \varphi_U^S + \varphi C_R^S \, , \tag{4.9}$$

where $\breve{\varphi}_U^S$ is the corrected rover carrier phase (cycles),

φ_U^S is the rover carrier phase observation (cycles),

φC_R^S is the carrier phase correction received from the reference station (cycles),

and

$$\breve{P}_U^S = P_U^S + C_R^S \, , \tag{4.10}$$

where $\breve{P}_U^S$ is the corrected rover pseudorange (metres),

P_U^S is the rover pseudorange observation (metres),

C_R^S is the pseudorange correction received from the reference station (metres).

This is analogous to differencing between receivers [i.e. Taveira-Blomenhofer and Hein, 1993]. By differencing the corrected carrier phase and pseudorange observations between satellites, double difference observations are formed. Satellite and receiver clock errors, in addition to orbital and atmospheric errors, can be eliminated or greatly reduced. Double difference ambiguities formed from equation (4.9) are different from the double difference ambiguities formed from the uncorrected carrier phase observations. This occurs because approximate integer ambiguities are included in the reference carrier phase observations when the phase corrections are generated (see equation (4.1)). The integer nature of the ambiguities is preserved, but the magnitude is changed. This causes no inconsistencies, since the ambiguities are estimated as parameters in both the floating ambiguity case and the fixed integer ambiguity solution presented in Chapter Three.

4.3 Data Transmission Formats

In developing the RTK GPS system for this research, two types of data transmission formats are used and comparisons of the transmission efficiencies are made. One is the

RTCM SC-104 format [RTCM, 1994], which is generally used in real-time differential GPS applications. The other transmission format is The U of C (The University of Calgary) format which is defined by the author for this research.

4.3.1 RTCM Type 18-21 Formats

RTCM version 2.1 defines data transmission formats for RTK GPS applications. RTCM message types 18-19 are for uncorrected carrier phase and pseudorange transmission, while types 20-21 are for the transmission of carrier phase and pseudorange corrections. The general RTCM message format includes a two-word header, followed by N data words, where N depends on message type as well as within a message type. Each word is 30 bits long. The two-word header format is common for each message type (see Figure 4.4), and the other N words contain data specific to the type of message transmitted.

In Figure 4.4, **STATION ID** refers to the identification of the differential reference station. **MODIFIED Z-COUNT** is the time of the start of the next frame (for pseudolite transmissions) as well as the reference time for the message parameters. **SQ NO.** means sequence number and **S/H** means station health. The detailed content of these two words can be found in RTCM version 2.1, while the parity encoding algorithm can be found in ICD-GPS-200 [1991].

FIRST WORD OF EACH MESSAGE

Bit 1 2 3 4 5 6 7 8 9 10 11 12 13 14 15 16 17 18 19 20 21 22 23 24 25 26 27 28 29 30

PREAMBLE 01100110	MESSAGE TYPE (FRAME ID)	STATION ID	PARITY

SECOND WORD OF EACH MESSAGE

Bit 1 2 3 4 5 6 7 8 9 10 11 12 13 14 15 16 17 18 19 20 21 22 23 24 25 26 27 28 29 30

MODIFIED Z-COUNT	SQ NO.	LENGTH OF FRAME	S/H	PARITY

Figure 4.4: Two-Word Header for All Message Types

a) Type 18-19 format

RTCM types 18-19 are data transmission formats for the uncorrected carrier phase and pseudorange observations. The first two words for each message type are shown in Figure 4.1, while Figures 4.5 and 4.6 show the remaining words for each of these two message types.

THIRD WORD

Bit 1 2 3 4 5 6 7 8 9 10 11 12 13 14 15 16 17 18 19 20 21 22 23 24 25 26 27 28 29 30

F	SP	GPS TIME OF MEASUREMENT	PARITY

EACH SATELLITE - 2 WORDS

Bit 1 2 3 4 5 6 7 8 9 10 11 12 13 14 15 16 17 18 19 20 21 22 23 24 25 26 27 28 29 30

H F	P C	R	SID	DQ	CUM. LOSS OF CONT.	CARRIER PHASE UPPER BYTE	PARITY

CARRIER PHASE LOWER THREE BYTES	PARITY

Figure 4.5: Type 18 - Uncorrected Carrier Phase Message Format

THIRD WORD

Bit 1 2 3 4 5 6 7 8 9 10 11 12 13 14 15 16 17 18 19 20 21 22 23 24 25 26 27 28 29 30

F	SM	GPS TIME OF MEASUREMENT	PARITY

EACH SATELLITE - 2 WORDS

Bit 1 2 3 4 5 6 7 8 9 10 11 12 13 14 15 16 17 18 19 20 21 22 23 24 25 26 27 28 29 30

SP	P C	R	SID	DQ	MULTIPATH ERROR	PSEUDORANGE UPPER BYTE	PARITY

PSEUDORANGE LOWER THREE BYTES	PARITY

Figure 4.6: Type 19 - Uncorrected Pseudorange Message Format

In Figures 4.5 and 4.6, the symbols are defined as follows:

F = Frequency Combination Indicator (L1, L2 or their combination),

SP = Spare,

H/F = Half/Full L2 Wavelength Indicator,

P/C = C/A-Code/P-Code Indicator,

R = Reserved for Future Expansion of Satellite ID,

SID = Satellite ID,

DQ = Data Quality (estimated one sigma phase measurement error),

CUM. LOSS OF CONT. = Cumulative Loss of Continuity Indicator (indicates unfixed cycle slip or loss of lock),

and **SM** = Smoothing Interval (indicates the interval for carrier smoothing of pseudorange data).

b) Type 20-21 formats

RTCM types 20-21 are data transmission formats for the carrier phase and pseudorange corrections. The first two words for each message type are shown in Figure 4.4, while Figures 4.7 and 4.8 show the remaining words for each of the two message types.

THIRD WORD

Bit 1	2 3	4 5 6 7 8 9 10 11 12 13 14 15 16 17 18 19 20 21 22 23 24	25 26 27 28 29 30
F	SP	GPS TIME OF MEASUREMENT	PARITY

EACH SATELLITE - 2 WORDS

Bit 1	2	3	4 5 6 7 8	9 10	11 12 13 14 15 16	17 18 19 20 21 22 23 24	25 26 27 28 29 30
H F	P C	R	SID	DQ	CUM. LOSS OF CONT.	ISSUE OF DATA	PARITY

CARRIER PHASE CORRECTION	PARITY

Figure 4.7: Type 20 - Carrier Phase Corrections Message Format

THIRD WORD

Bit 1	2 3	4 5 6 7 8 9 10 11 12 13 14 15 16 17 18 19 20 21 22 23 24	25 26 27 28 29 30
F	SM	GPS TIME OF MEASUREMENT	PARITY

EACH SATELLITE - 2 WORDS

Bit 1	2	3	4 5 6 7 8	9	10 11 12 13	14 15 16 17 18 19 20 21 22 23 24	25 26 27 28 29 30
SP	P C	R	SID	P R S F	DQ	MULTIPATH ERROR	ISSUE OF DATA	PARITY

PSEUDORANGE CORRECTION	RANGE RATE CORRECTION	PARITY

Figure 4.8: Type 21 - Pseudorange Corrections Message Format

In Figures 4.7 and 4.8, the symbols are defined as in Figures 4.5 and 4.6, with the addition of

PRSF = Pseudorange Correction Scale Factor (an indicator relating to the data quality encoding algorithm, details in RTCM version 2.1).

For each RTCM type 18-21 message, the total number of words is 3+2n, where n is the number of satellites. The number of bytes is computed as $(3+2n) \times 30/8$. For example, if six satellites are available, then 57 bytes need to be transmitted.

4.3.2 The U of C Formats

RTCM message formats are standard public formats available to all GPS users. Generating the standard RTCM formatted message at the reference station is complicated, since the 30-bit word type is not an ordinary data type for computers. Additionally, the user cannot add or delete information. For single users who control both the reference station and the rover, it may therefore be more convenient for them to define their own formats. The U of C formats for transmission of observations, as well as corrections, were defined by the author during the development of the system in this thesis.

a) The U of C format for uncorrected observations

In The U of C format, Doppler observations are transmitted in addition to carrier phase and pseudorange observations. Doppler observations are therefore available for determining the velocity of the rover. This is beneficial for determination of the rover velocity, since the Doppler observations are directly related to the rover velocity (see the observation equation 2.9 in Chapter Two). The U of C format is defined as follows:

$GPS Time, Number of Satellites, Satellite ID, Pseudorange, Doppler, Carrier Phase, ..., Satellite ID, Pseudorange, Doppler, Carrier Phase, \r\n.

This is a simple ASCII format in which the data can be put into the buffer of a serial port one character at a time. The ASCII data are separated by commas, while \r and \n are the return and new line symbols, respectively. There are no extra parity bits included in the format. Transmission errors are detected at the rover by comparing the number of commas received with the number of commas computed (where number of commas computed = number of satellites $\times$ 4 + 2). If the two numbers are different, a transmission error is assumed to have occurred.

The total number of bytes in The U of C format depends on the number of satellites and the range of the observation values. Ordinarily, if six satellites are available, approximately

180 bytes must be transmitted. This number of bytes is larger than the number of bytes for RTCM types 18-19 (114 bytes), since raw observations in The U of C format are larger numbers (raw carrier phase and pseudorange measurements) and Doppler observations are included in The U of C format.

b) The U of C format for corrections

A U of C format was also developed for transmission of carrier phase and pseudorange corrections:

$GPS Time, Number of Satellite, Satellite ID, Pseudorange Correction, Carrier Phase Correction, ..., , Satellite ID, Pseudorange Correction, Carrier Phase Correction, \r\n

There are no extra parity bits included in the format. Transmission errors are detected using the method described in **a)** above.

The magnitude of correction values is much smaller than that of uncorrected observations. If six satellites are available, approximately 90 bytes must be transmitted. This number of bytes is smaller than the number of bytes for RTCM types 20-21 (114 bytes), and is much smaller than the number of bytes required for raw data transmission using The U of C format (180 bytes).

CHAPTER FIVE

SYSTEM COMPONENTS AND INTEGRATION

5. 1 Hardware Components

The RTK DGPS system is composed of two GPS receivers, two portable computers and a pair of radio transceivers. The configuration of the system is shown in Figure 5.1.

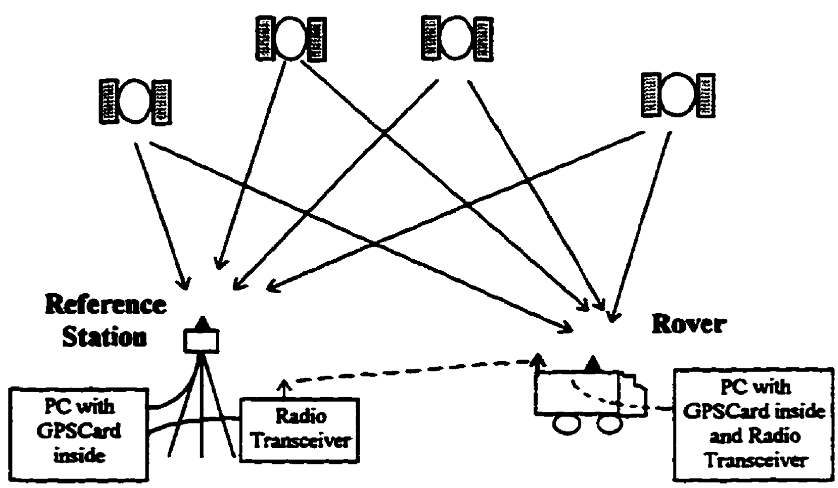

Figure 5.1: System Configuration

5.1.1 GPS Receivers

Two L1 C/A code NovAtel GPSCard™ receivers (either 10 or 12 channel units) were used in this system. Making use of Narrow Correlator [Fenton et al., 1991] technology, the NovAtel GPS receivers provide a pseudorange resolution of 10 cm. The GPSCard™ was plugged directly into the ISA slot of a laptop computer. The NovAtel geodetic antenna (model 501) and accompanying choke rings were used to obtain high accuracy observations and minimize multipath effects, which is beneficial to ambiguity resolution.

The system can also be adapted to use two NovAtel OEM GPS sensors in place of the two NovAtel GPSCard™ receivers. Each OEM GPS sensor can be connected to one of the serial ports of a laptop computer using a standard RS-232 cable. The laptop computer therefore requires at least two serial ports for such a system, in order to connect with an OEM GPS sensor and a radio transceiver.

5.1.2 Laptop Computers

A laptop computer was required at both reference and the rover sites. At the reference station, a Compaq 386 was used to generate the corrections while a Grid 486 was used at the rover to generate real-time solutions, since many computations were required at the rover end. A large space hard disk was required for each computer. Raw data was recorded at 1 Hz, which translates into approximately 3 Megabytes of ASCII data per hour.

5.1.3 Radio Transceivers and Power Supply

A pair of Hopper™ radio transceivers were also used in the system [Hopper™, 1994]. These transceivers are wireless modems for mobile users which operate at speeds up to 38.4 kps in the 902~928 MHz unlicensed spread spectrum band, with 1 W transmit power. The maximum transmission range is specific 30 km for a clear line of sight.

Twelve volt DC batteries supplied power to both the transceivers and computers, while the battery in the rover vehicle provided an alternate source of power.

5. 2 Software Development

5.2.1 Modifications to FLYKIN™

Software developed for the real-time system is based on FLYKIN™, a suite of C programs developed at The University of Calgary designed to process GPS differential carrier phase data in both kinematic and static modes [Lu and Cannon, 1994]. These programs include OTF double difference carrier phase integer ambiguity resolution, forward- and reverse-time kinematic positioning, and statistical testing of carrier phase residuals. The OTF ambiguity resolution algorithm is based on the FASF technique described in Chapter Three.

Since FLYKIN™ is a post-processing program, many modifications were necessary to conduct real-time positioning. Modifications are listed as follows:

1) Data communication between the laptop computers and receivers was implemented by the author. FLYKIN™ obtains GPS observations by reading data files. For this real-time system, GPS observations are obtained directly from the receivers at a 1 Hz update rate. Computer routines necessary for communication between the computers and the GPSCard™ receivers were provided by NovAtel, while serial communication routines, developed by Terry Labach at The University of Calgary, were used for communication with the OEM GPS sensors.

2) Real-time data logging and preprocessing functions were added by the author. Raw data from the GPS receivers are initially logged at a 1 Hz update rate, and then decoded and transformed into a format compatible with pre-existing FLYKIN™ routines.

3) Data communication between the laptop computers and the radio transceivers was implemented by the author. For this system, the uncorrected observations or corrections

are transmitted from the reference station to the rover by a pair of radio transceivers. The data communication between the laptop computers and the radio transceivers was realized by using serial communication routines developed by Terry Labach at The University of Calgary.

4) A group of routines were added by the author to generate the carrier phase and pseudorange corrections described in Chapter Four.

5) A group of routines were added to encode the raw observations and their corrections into RTCM types 18-21 formats and The University of Calgary formats (defined in Chapter Four by the author).

6) FLYKIN™ was modified by the author to process carrier phase and pseudorange corrections, as well as raw Doppler observations.

7) The option of a floating ambiguity solution was added by the author. FLYKIN™ outputs the differential carrier phase-smoothed code solutions prior to fixing the carrier phase integer ambiguities. Once the integer ambiguities are fixed, kinematic positions of the rover are computed using double difference carrier phase observations only. In this system, if the floating ambiguity solution option is chosen, the system outputs floating ambiguity solutions without fixing the integer ambiguities. If the integer ambiguity

solution option is chosen, the system first outputs floating ambiguity solutions prior to fixing integer ambiguities, and integer ambiguity solutions are then output once the integer ambiguities are fixed.

8) Statistical testing, based on the innovation sequence, was added by the author, in order to implement quality control of the floating ambiguity solution.

5.2.2 System Data Processing

A flowchart illustrating data processing for the real-time system is shown in Figure 5.2. At the reference station, raw GPS data (i.e. ephemeris, pseudorange, Doppler and carrier phase data) are downloaded from the receiver and preprocessed in the portable computer. If uncorrected observations are required at the rover, the uncorrected observations (carrier phase, pseudorange or Doppler observations) are transmitted by the radio transceivers. Otherwise, pseudorange and carrier phase corrections are generated, using the known location of the reference station as input, and transmitted by the radio transceivers (see Figure 5.2). It is assumed that precise reference station coordinates are available for computations at the rover, if raw observations have been transmitted. Precise reference station coordinates may be transmitted in an RTCM type 3 message [RTCM, 1994] or in an alternative message, defined by the user.

At the rover, raw GPS data are also downloaded from the receiver and preprocessed in the computer. After preprocessing the raw data, uncorrected observations (or corrections) received from the reference station are downloaded from the radio transceiver buffer. If the received data consist of uncorrected observations, the observations are first processed to reject any selected satellites. Satellite coordinates are then computed, and the satellite observations retained only if the satellite elevation angle exceeds the specified mask angle. Tropospheric corrections are then applied to each observation, a base satellite is chosen, and cycle slips are detected. The same data processing steps are applied to the rover observations. If the received data consist of corrections generated at the reference station, the corrections are input directly into the floating ambiguity solution at the rover, since the observations used to generate these corrections have already been processed at the reference station (see Figure 5.2).

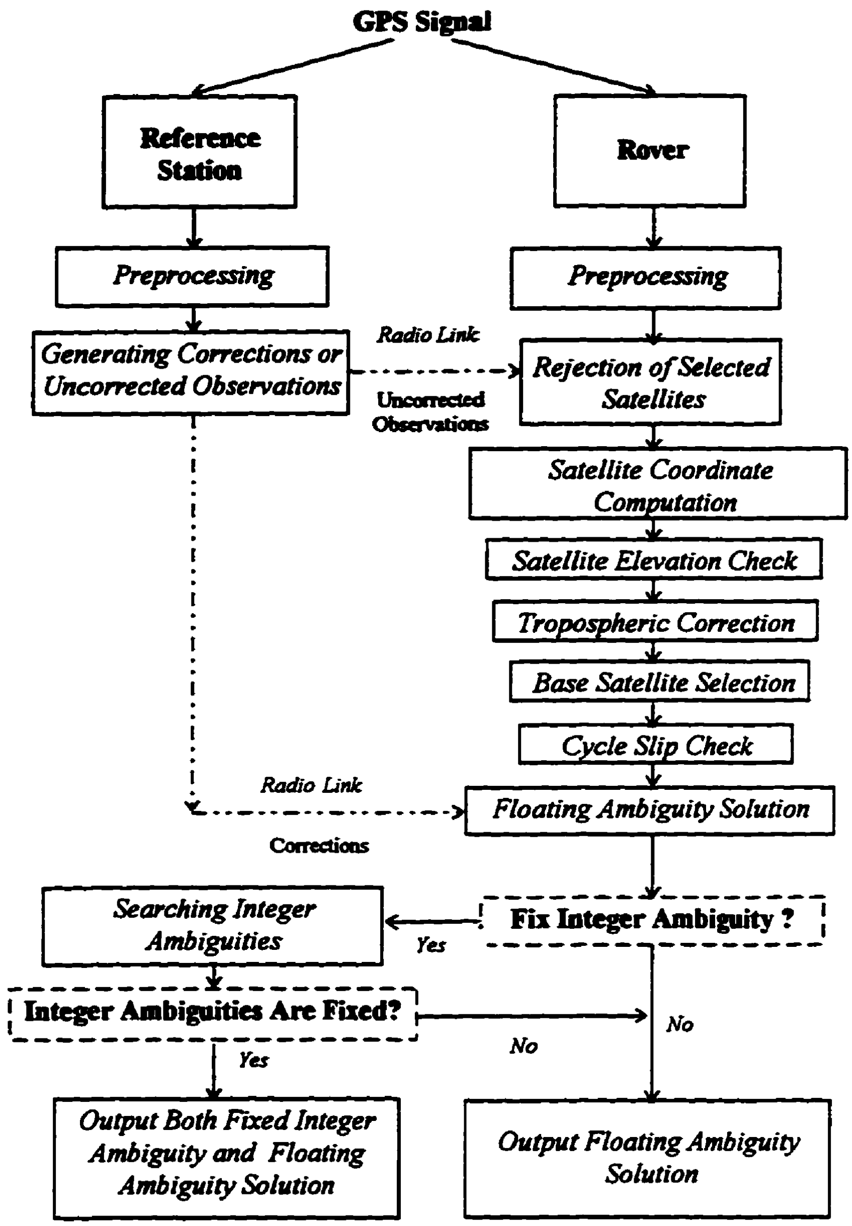

Figure 5.2: Data Processing in the System

The rover GPS data are corrected using either the uncorrected observations or corrections generated at the reference receiver, such that single differences between the reference and the rover observations are formed for each satellite in common view. Double differences between satellites are then formed and used as input into the floating ambiguity solution, followed by the fixed integer ambiguity solution. The carrier phase double difference ambiguities are estimated as floating (i.e. real) numbers initially, at which point the system outputs floating ambiguity solutions. If fixed integer ambiguity solutions are required, the system will then search for the correct integer ambiguities. Once the integer ambiguities are fixed, fixed integer ambiguity solutions are output, in addition to the floating ambiguity solutions (see Figure 5.2).

5.2.3 Time-Matching Technique

To achieve the highest degree of accuracy, rover observations should be synchronized with data transmitted by the reference station, such that major error sources can be eliminated or greatly reduced through double difference processing. Because of the transmission and serial port delays, rover observations may not be synchronized with incoming data from the reference station. This causes inaccuracies in the rover position solutions. Time-matching of the rover and reference data sets is employed to solve the problem. Both the rover observations and the data transmitted by the reference station are tagged with values of the GPS time at a 1 Hz update rate. The rover and reference data sets can then be synchronized using their GPS time tags (Figure 5.3).

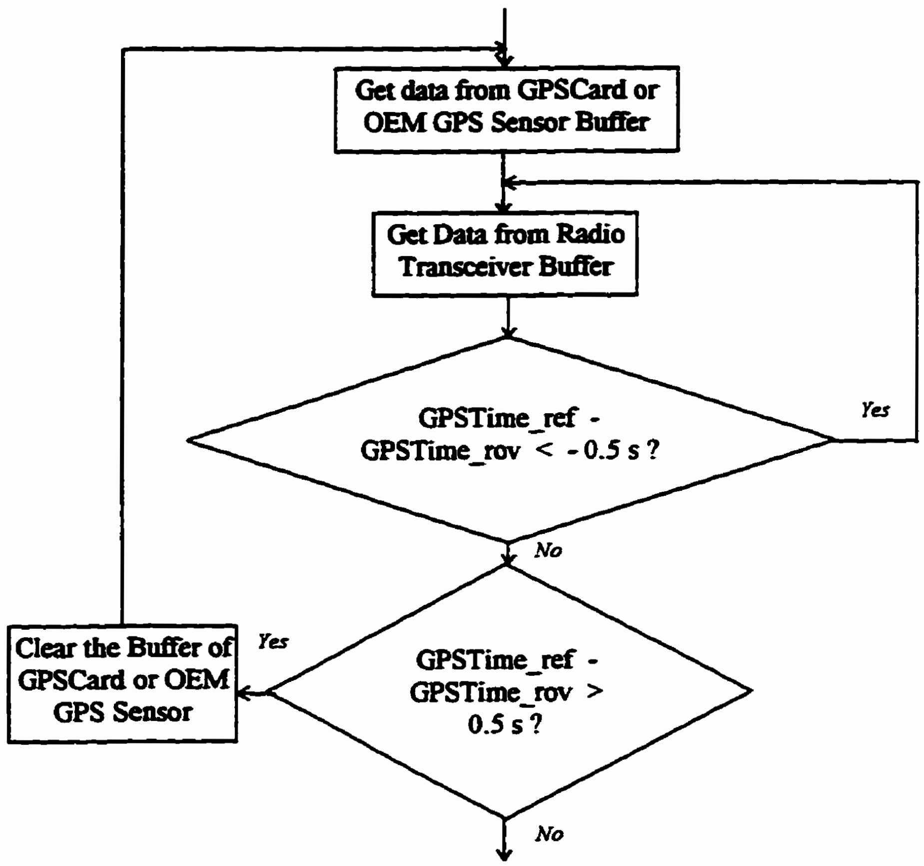

Figure 5.3: Time-Matching Procedure

In Figure 5.3, GPSTime_ref refers to the GPS time tag for data received from the reference station while GPSTime_rov refers to the GPS time tag for rover observations. If the received data are delayed, the program will choose reference data from the next epoch, as stored in the radio transceiver buffer. If the rover data are delayed, the program will clear the buffer, skip the present epoch, and begin the algorithm again at the next epoch.

clear the buffer, skip the present epoch, and begin the algorithm again at the next epoch. After the rover and received data are synchronized, the program will process the data and compute position solutions.

For this system, the time latency of the corrections and the raw observations is approximately 0.4 and 0.5 seconds, respectively, using The U of C formats, and about 0.4 seconds using the RTCM formats (when a baud rate of 9600 bps is used). The rover position results are output about 0.6 seconds after the observations are measured [Lan and Cannon, 1996]. The system developed here is therefore a 'quasi' real-time system.

To achieve 'real' real-time position, the integer ambiguities are resolved using time-matched observations first. Then the received carrier phase observations or corrections from the reference station can be predicted to the current time. The current rover carrier phase observations are processed with the predicted observations using the known integer ambiguities [Newmann et. al., 1996]. Another approach is to predict the current position using the previous position and velocity.

CHAPTER SIX

SYSTEM QUALITY CONTROL

Quality control is an essential component of the RTK GPS system, ensuring that the system is functioning properly. In post-mission, the GPS data can be processed in both forward and reverse modes or data smoothing can be implemented, to reduce the effects of undetected errors and to obtain optimal positioning results. For a real-time system, the positioning results must be generated in real-time and, hence, undetected errors may cause large positioning errors [Wei et al., 1990]. This chapter introduces some statistical methods for quality control of both the floating and fixed integer ambiguity solutions.

6.1 Quality Control of the Floating Ambiguity Solution

As described in Chapter Two, the floating ambiguity solution estimates the position and velocity vectors, as well as the floating ambiguities, using a Kalman filter. The innovation sequence, i.e. predicted residuals, are widely used for quality control of Kalman filtering [Teunissen, 1990; Lu and Lachapelle, 1990; Wei et al., 1990]. The innovation sequence is therefore used in this RTK GPS system for quality control of the floating ambiguity solution.

6.1.1 Biased Kalman Filter

Table 6.1 shows the standard Kalman Filter estimation equations, as presented in Appendix.

Table 6.1: Standard Kalman Filter Equations

System Model Observation Model	$\mathbf{x}_{k+1} = \mathbf{\Phi}_{k+1,k}\mathbf{x}_k + \mathbf{w}_k, \qquad \mathbf{w}_k \sim N(0, \mathbf{C}_k^w)$ $\mathbf{z}_{k+1} = \mathbf{H}_{k+1}\mathbf{x}_{k+1} + \varepsilon, \qquad \varepsilon \sim N(0, \mathbf{C}_\varepsilon)$
Prediction	$\mathbf{x}_{k+1}(-) = \mathbf{\Phi}_{k+1,k}\mathbf{x}_k(+)$ $\mathbf{C}_{k+1}^x(-) = \mathbf{\Phi}_{k+1,k}\mathbf{C}_k^x(+)\mathbf{\Phi}_{k+1,k}^T + \mathbf{C}_{k+1}^w$
Update	$\mathbf{x}_{k+1}(+) = \mathbf{x}_{k+1}(-) + \mathbf{K}\left[\mathbf{z}_{k+1} - \mathbf{H}_{k+1}\mathbf{x}_{k+1}(-)\right]$ $\mathbf{C}_{k+1}^x(+) = \left[\mathbf{I} - \mathbf{K}\mathbf{H}_{k+1}\right]\mathbf{C}_{k+1}^x(-)$ $\mathbf{K} = \mathbf{C}_{k+1}^x(-)\mathbf{H}_{k+1}^T\left[\mathbf{H}_{k+1}\mathbf{C}_{k+1}^x(-)\mathbf{H}_{k+1}^T + \mathbf{C}^\varepsilon\right]^{-1}$

In Table 6.1, the updated state vector $\mathbf{x}_{k+1}(+)$ is an unbiased solution with minimum variance under the normal operation conditions, i.e.

$$\mathbf{w}_k \sim N(0, \mathbf{C}_k^w) \qquad\qquad \varepsilon \sim N(0, \mathbf{C}_\varepsilon)$$

and no cross correlation between $\mathbf{w}_k$ and ε. This is often regarded as hypothesis H_0 or the null hypothesis. An alternative hypothesis is the constant bias hypothesis H_a. When a constant bias vector **b**, of unknown magnitude is present in the system or observation model of a Kalman filter, the system and observation model in Table 6.1 can be reformulated as:

$$\mathbf{x}_{k+1} = \mathbf{\Phi}_{k+1,k}\mathbf{x}_k + \mathbf{B}_{k+1}\mathbf{b} + \mathbf{w}_k , \tag{6.1}$$

and $$\mathbf{z}_{k+1} = \mathbf{H}_{k+1}\mathbf{x}_{k+1} + \mathbf{D}_{k+1}\mathbf{b} + \varepsilon , \tag{6.2}$$

where the matrices $\mathbf{B}_{k+1}$ and $\mathbf{D}_{k+1}$ determine how the components of the bias vector **b** enter the system and observation models, respectively.

Then the prediction and update equations will become

$$\mathbf{x}_{k+1}(-) = \mathbf{\Phi}_{k+1,k}\mathbf{x}_k(+) + \mathbf{B}_{k+1}\mathbf{b} \tag{6.3}$$

and $$\mathbf{x}_{k+1}(+) = \mathbf{x}_{k+1}(-) + \mathbf{K}\left[\mathbf{z}_{k+1} - \mathbf{H}_{k+1}\,\mathbf{x}_{k+1}(-) - \mathbf{D}_{k+1}\mathbf{b}\right] \tag{6.4}$$

The constant bias hypothesis H_a is used in quality control of the floating ambiguity solution.

6.1.2 Innovations Sequence

If the null hypothesis is true, standard Kalman filter equations (Table 6.1) give the minimum-variance, unbiased estimate of the state vector at each epoch. In this case, the innovation sequence $\mathbf{v}_{k+1}$ can be derived as

$$\mathbf{v}_{k+1} = \mathbf{z}_{k+1} - \mathbf{H}_{k+1}\,\mathbf{x}_{k+1}(-)\,. \tag{6.5}$$

This is a zero-mean, Gaussian white noise sequence, with a variance-covariance matrix:

$$\mathbf{C}_{v_{k+1}} = \mathbf{C}_{\varepsilon} + \mathbf{H}^{T}\mathbf{C}^{x}_{k+1}(-)\mathbf{H}\,. \tag{6.6}$$

If hypothesis H_a is true, the innovations sequence can be derived from equations (6.1), (6.2) and (6.3) as

$$\mathbf{v}_{k+1} = \mathbf{z}_{k+1} - \mathbf{H}_{k+1}\,\mathbf{x}_{k+1}(-) + \mathbf{S}_{v_{k+1}}\mathbf{b}\,, \tag{6.7}$$

where $\mathbf{S}_{v_{k+1}} = \mathbf{D}_{k+1} - \mathbf{H}_{k+1}\mathbf{B}_{k+1}\,.$ (6.8)

In this case, the innovations sequence (6.7) will depart from zero-mean and lose its white noise properties. The innovations sequence is therefore an ideal residual sequence for detecting abnormal system behavior.

6.1.3 Statistical Testing and Bias Recovery

Statistical testing of the null hypothesis H_0, against the alternative hypothesis H_a, is used to detect and identify possible biases in the filter. In this real-time system, the statistical testing is called "local testing" because only the innovation vector $\mathbf{v}$ from the current epoch is used.

System biases are initially unknown. To detect an unspecified system bias, a simple Chi-squared test is performed on the innovations sequence [Teunissen, 1990; Wei et al., 1990] :

$$T^1 = \mathbf{v}^T C_v^{-1} \mathbf{v} \sim \chi^2(m, 0), \qquad \mathbf{v} \sim N(0, C_v) \quad \text{under } H_0 \tag{6.9}$$

where m is the dimension of $\mathbf{v}$.

Under a certain level of significance α ($\alpha = 0.05$ here), the bias detection test is performed according to the following criteria:

$$\begin{aligned} T^1 &< \chi^2_\alpha, && \text{no bias,} \\ T^1 &\geq \chi^2_\alpha, && \text{biases occurred.} \end{aligned} \tag{6.10}$$

Once the biases are detected, the bias identification process is conducted. An approach similar to data-snooping [Baarda, 1968] is employed to identify the biases [Teunissen and Salzman, 1989]:

$$T^2 = \frac{\left(S_v^T C_v^{-1} v\right)^2}{S_v^T C_v^{-1} S_v} \sim \chi^2(1,0) \quad \text{under } H_0 . \tag{6.11}$$

Here S_v is a one dimensional vector, computed from equation (6.8) under the assumption that only one bias has occurred. For example, D_{k+1} is chosen as

$$D_{k+1} = \left(\underset{1}{0}, \ldots, 0, \underset{i}{1}, 0, \ldots, \underset{m}{0}\right)^T . \tag{6.12}$$

in equations (6.2) and (6.8), where i is assigned a value i = 1, 2, ..., m, and each observation is tested in turn to search for biased values.

In RTK GPS, the most common and severe biases are carrier phase cycle slips, which are multiples of the carrier phase wavelength (λ_{L_1} = 19.02 cm). The statistical methods described above are suitable for cycle slip detection and identification [Lu and Lachapelle, 1990; Wei et al., 1990] and were implemented in this RTK GPS system.

Unfortunately in some cases, especially for large or multiple biases, the above identification test is too sensitive, identifying more biases than are actually present. Such cases were encountered by both the author and Lu and Lachapelle [1990]. To overcome or alleviate this problem, the minimum detectable bias (MDB) is used to confirm the identified bias. The MDB value b_0 for each error source is computed as

$$b_0 = \sqrt{\frac{\lambda_0}{S_v^T C_v^{-1} S_v}} \; . \tag{6.13}$$

Here $\sqrt{\lambda_0}$ is the minimum value of the non-centrality parameter which satisfies the given test power $1-\beta_0$ and significance level α.

If a bias in the observation z_i is identified by equation (6.11), the innovations residual v_i is derived from equation (6.7) as

$$v_i = z_i - \mathbf{H}_i \mathbf{x}_{k+1}(-) + b_i \; . \tag{6.14}$$

It is evident that the bias b_i is directly absorbed by the corresponding innovation v_i. Therefore, the confirmation is performed by comparing MDB value b_0 with v_i, where

$$|v_i| \geq b_0, \qquad \text{correct identification,}$$

or $|v_i| < b_0,$ wrong identification.

When a bias is identified and confirmed, bias recovery is performed by rejecting the biased observations, and recomputing the least squares estimation.

6.2 Quality Control of the Fixed Integer Ambiguity Solution

Once the integer ambiguities are fixed, positions with centimetre level accuracies are obtained in a simple least squares estimation, using double difference carrier phase observations. The residuals $\hat{\mathbf{v}}$ and corresponding variance-covariance matrix $\mathbf{C}_{\hat{\mathbf{v}}}$ can be derived from equations (3.25)-(3.27) in Chapter Three as

$$\hat{\mathbf{v}} = -\mathbf{C}_{\hat{\mathbf{v}}}\, \mathbf{C}^{\varepsilon^{-1}}\mathbf{w}, \tag{6.15}$$

$$\mathbf{C}_{\hat{\mathbf{v}}} = \mathbf{C}^{\varepsilon} - \mathbf{H}\left[\mathbf{H}^T\mathbf{C}^{\varepsilon^{-1}}\mathbf{H}\right]^{-1}\mathbf{H}^T. \tag{6.16}$$

If no bias has occurred in the observation vector $\mathbf{l}$ (hypothesis H_0), the residual $\hat{\mathbf{v}}$ statistically resembles Gaussian distribution with zero mean: $\hat{\mathbf{v}} \sim N(0, \mathbf{C}_{\hat{\mathbf{v}}})$. If biases have occurred (hypothesis H_a), $\hat{\mathbf{v}}$ has a Gaussian distribution with non-zero mean: $\hat{\mathbf{v}} \sim N(\mathbf{w}_0, \mathbf{C}_{\hat{\mathbf{v}}})$. The MDB value b_i, corresponding to the observation l_i, is computed by the equation

$$b_i = \sigma_{l_i}\sqrt{\frac{\lambda_0}{g_i}} \quad , \tag{6.17}$$

where σ_{l_i} is the standard deviation of l_i (metre),

$\sqrt{\lambda_0}$ is the minimum value of the non-centrality parameter which satisfies the given test power $1-\beta_0$ and significance level α ,

and g_i is the i[th] diagonal element of $\mathbf{G} = \mathbf{C}_{\hat{v}}\mathbf{C}_l^{-1}$.

If a bias Δl_i has occurred in l_i, the effect of the bias on the residual v_i is derived from equation (6.15) as

$$v_i = -g_i \Delta l_i \quad . \tag{6.18}$$

This equation can be manipulated to estimate the bias Δl_i by

$$\Delta l_i = -\frac{v_i}{g_i} \quad . \tag{6.19}$$

Assuming that only one bias has occurred, it can be detected and identified using a data snooping process, in which Δl_i values are compared with their corresponding MDB values b_i, one at a time [Baarda, 1968]. This process enables the system to detect and identify double difference cycle slips in the integer ambiguity solution. Once a cycle slip has been detected and identified, the system will reject the related observation and recompute the least squares estimation. The new position estimate is used to compute a new ambiguity for the biased double difference carrier phase observation.

The quality control methods for both floating ambiguity solution and fixed integer ambiguity solution are based on the assumption that only one bias occurs at a given epoch. In case of two or more biases, the methods described here may not work well. More research should be done to handle the multi-bias situation. Simulations of single and two biases using static data are shown in Chapter Seven.

In addition to the data snooping method, the integer ambiguity and floating ambiguity solutions are compared at each epoch. If differences between the two position solutions are larger than predefined thresholds (0.5 m for the latitude and longitude components, and 1.0 m for the height component), the system will reinitialize the integer ambiguity search.

CHAPTER SEVEN

SYSTEM PERFORMANCE AND TEST RESULTS

To evaluate the performance of the system, various tests were conducted. Static tests were done at The University of Calgary, and two kinematic tests were performed, one on a farm in southern Alberta and another was done in Springbank near Calgary.

7.1 Static Tests

On the roof of the Engineering Building at The University of Calgary, there are pillars whose relative coordinates in WGS-84 are precisely known to the 1 cm level (see Figure 7.1). Pillars N1 and N2, spaced 3 m apart, were selected for the tests. Two NovAtel antennas were used with choke rings on each pillar.

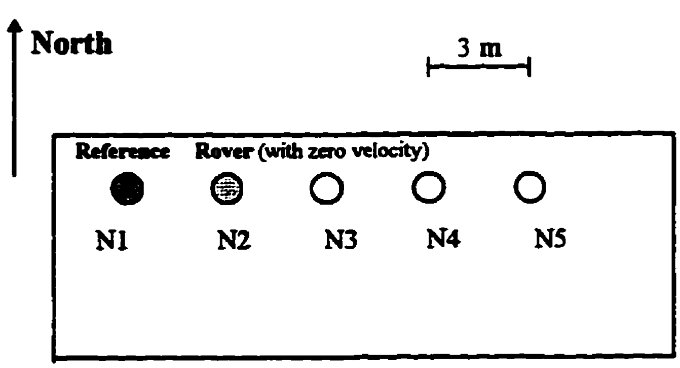

Figure 7.1: Sketch of The U of C Pillars

Before the performance tests of the system, many tests were done using different formats (described in Chapter Four) for real-time data transmission. No difference among the positioning results was found when different formats were used. For the later tests, The U of C format for carrier phase and pseudorange corrections was used considering the transmission efficiency (see Chapter Four).

The real-time carrier phase and pseudorange corrections were generated using the precise coordinates of Pillar N1. The coordinates of Pillar N2 were then output by the system in real-time, at a rate of 1 Hz. The real-time positions were compared with the known coordinates of Pillar N2, and the system performance was evaluated by considering the computed differences.

7.1.1 Short Time Period Test

The short time period test was conducted on September 19, 1995, and the test period was approximately 2 hours. Two NovAtel GPSCard™ receivers were used. Both floating ambiguity and fixed integer ambiguity solutions were computed. Five to seven satellites (in common) were tracked and the cut-off angle was chosen as 10°. The PDOP values were less than 3.0 throughout, and the number of satellites and PDOP values are shown in Figure 7.2.

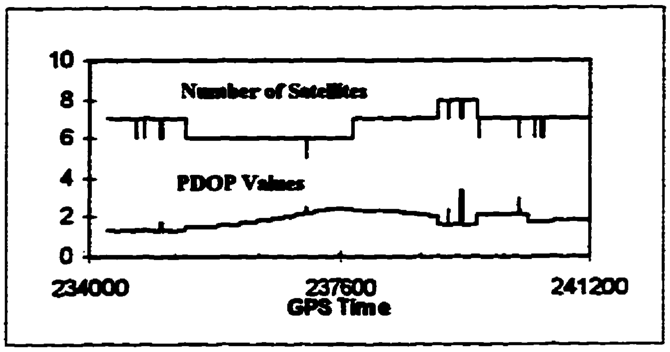

Figure 7.2: Satellite Number and PDOP (Short Baseline, Short Time Period Test)

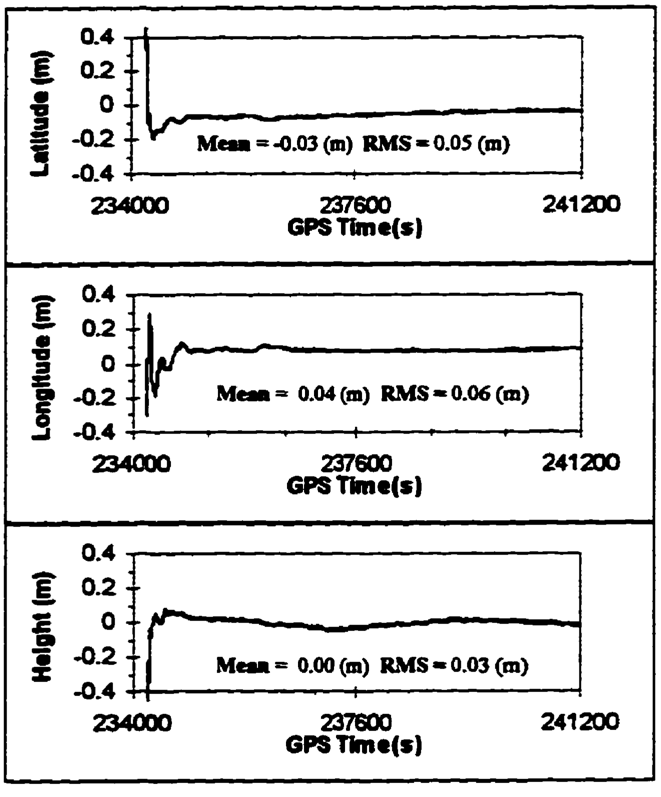

Figure 7.3: Performance of the Real-Time Floating Ambiguity Solution in Static Mode (Short Baseline, Short Time Period Test)

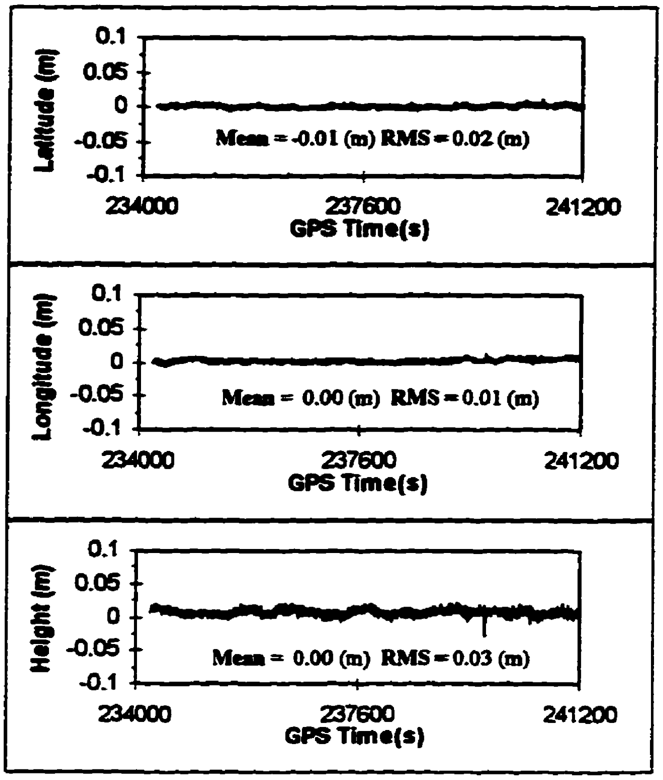

Figure: 7.4 Performance of the Real-Time Fixed Integer Ambiguity Solution in Static Mode (Short Baseline, Short Time Period Test)

For this test, the floating ambiguities converged quickly to accurate values, since the mean and RMS statistics reflect that the floating ambiguity position components are almost at the same accuracy level as the fixed integer ambiguity position components. Results are shown in Figures 7.3 and 7.4.

The integer ambiguity search was very effective and it took only 8 epochs (8 s) for FASF to fix the integer ambiguities, since seven satellites were available at the beginning of the test. Additionally, the baseline length was only 3 m, which is an important factor for OTF processing, since orbital and atmospheric errors are virtually eliminated by the double difference process for the short reference-rover distance in this case (see Figure 7.4).

7.1.2 Long Time Period Test

The objective of the long time period test was to determine if the system results remained consistent over many hours. A fourteen hour test was conducted on February 21, 1996, during which time 5 to 9 satellites were tracked. Two NovAtel GPSCard™ receivers were used. A cut-off angle of 10° was chosen and PDOP values were less than 3.0. The number of satellites and PDOP values are shown in Figure 7.5. Results of the real-time floating ambiguity solution, as well as the fixed integer ambiguity solution, are shown in Figures 7.6 and 7.7, respectively.

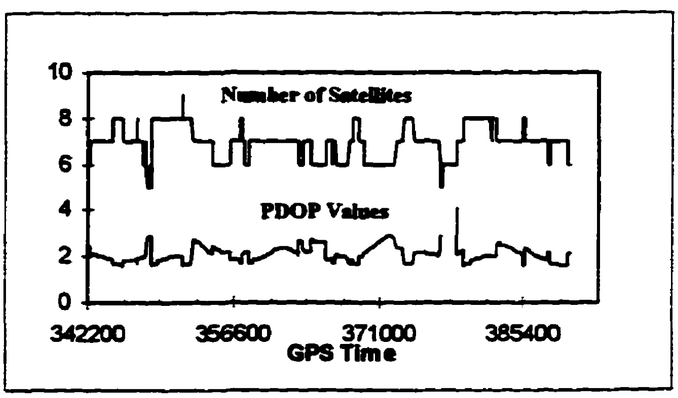

Figure 7.5: Satellite Number and PDOP (Short Baseline, Long Time Period Test)

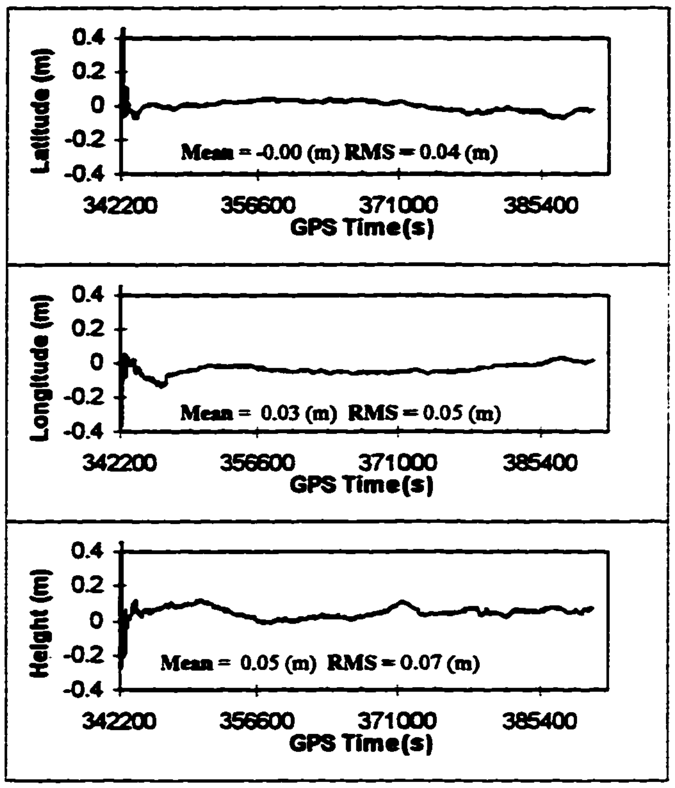

Figure 7.6: Performance of the Real-Time Floating Ambiguity Solution in Static Mode (Short Baseline, Long Time Period Test)

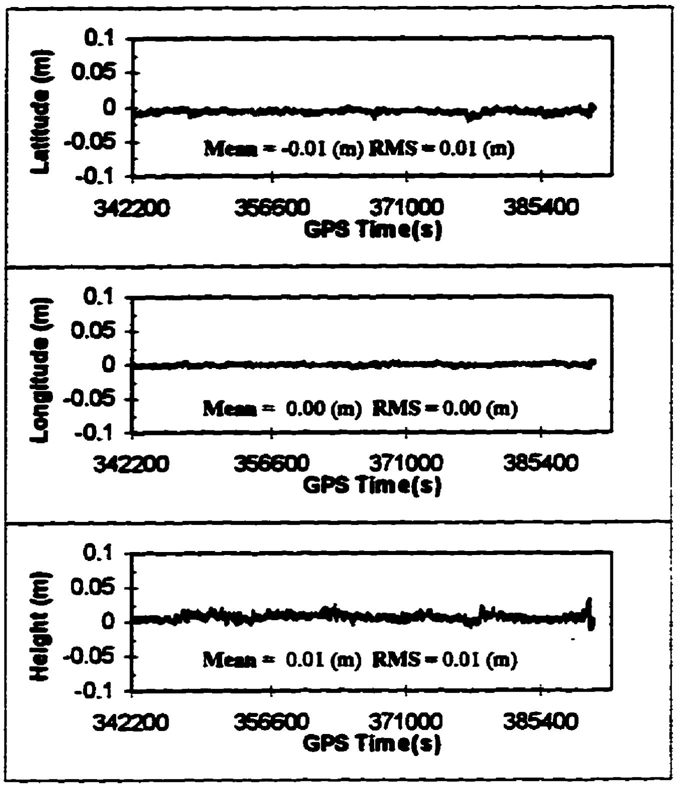

Figure 7.7: Performance of the Real-Time Fixed Integer Ambiguity Solution in Static Mode (Short Baseline, Long Time Period Test)

The system worked well throughout the 14 hour period. Both the floating ambiguity and fixed integer ambiguity solutions had a high degree of accuracy. RMS values for the floating ambiguity solutions are 0.04 m, 0.05 m, and 0.07 m for the latitude, longitude and height coordinate component, respectively. For the integer ambiguity solutions, the mean values agree to the known coordinates of the pillar within the uncertainty level of ± 1 cm. The magnitudes of the RMS values for the fixed integer ambiguity solutions are equal to the magnitudes of their mean values. This implies that the RMS values would be zero if there was no constant differences between the integer ambiguity solutions and the precise known coordinates.

7.1.3 Quality Control Simulations

To verify the quality control methods described in Chapter Six, single bias and two biases situations were simulated in post process mode. A set of data taking from the long time static test was used. The data is from GPS epoch 342400 to 344200. Seven satellites (12, 26, 2, 15, 27, 7, 9) are above 10° cut-off angle (see Figure 7.5). Satellite 12 with highest elevation angle was chosen as base satellite by the system.

Carrier phase cycle slip is the worst bias for the RTK system. Fortunately, the large cycle slips can be detected by Doppler observations in the cycle slip detection routine. There may be small cycle slips which cannot be detected. To simulate the single bias situation, one cycle bias was added to the observations of Satellite 15 beginning at GPS epoch 343400. The post-processed results (floating ambiguity and fixed integer ambiguity solution) were compared to known coordinates of Pillar N2. The differences were used to evaluate the performance of both floating ambiguity and fixed integer ambiguity solution when single bias happens (see following figures).

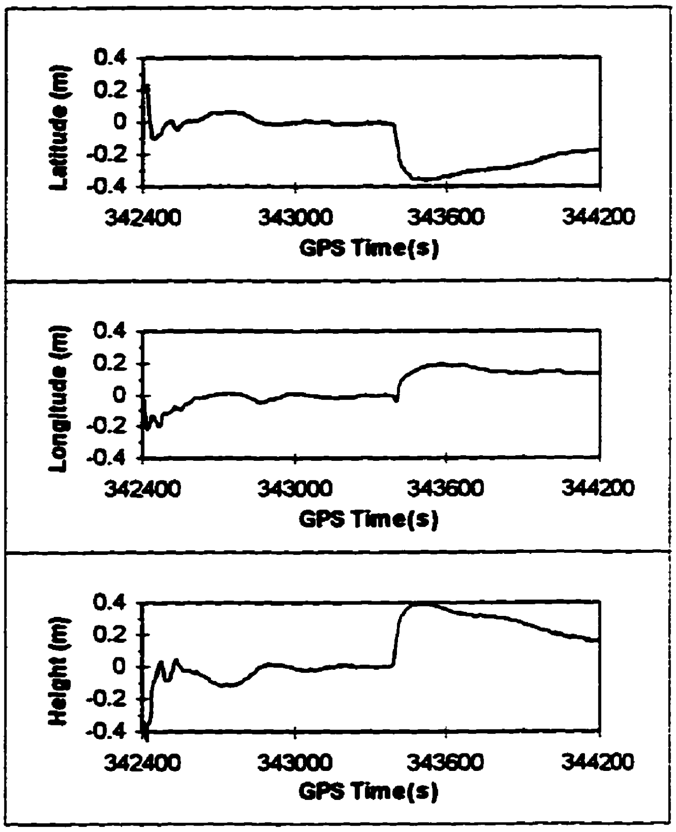

Figure 7.8: Performance of the Floating Ambiguity Solution without Quality Control (Single Bias Situation)

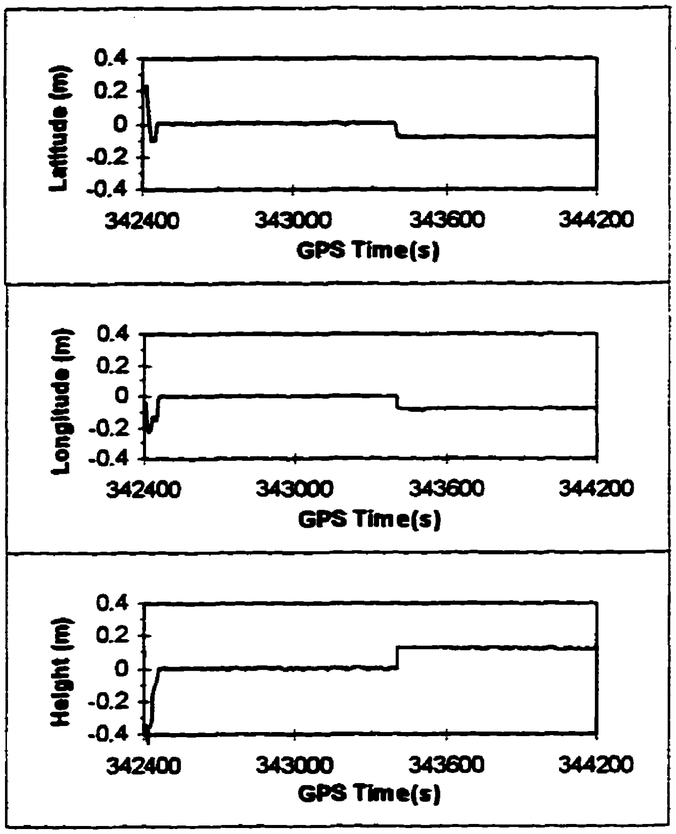

Figure 7.9: Performance of the Fixed Integer Ambiguity Solution without Quality Control (Single Bias Situation)

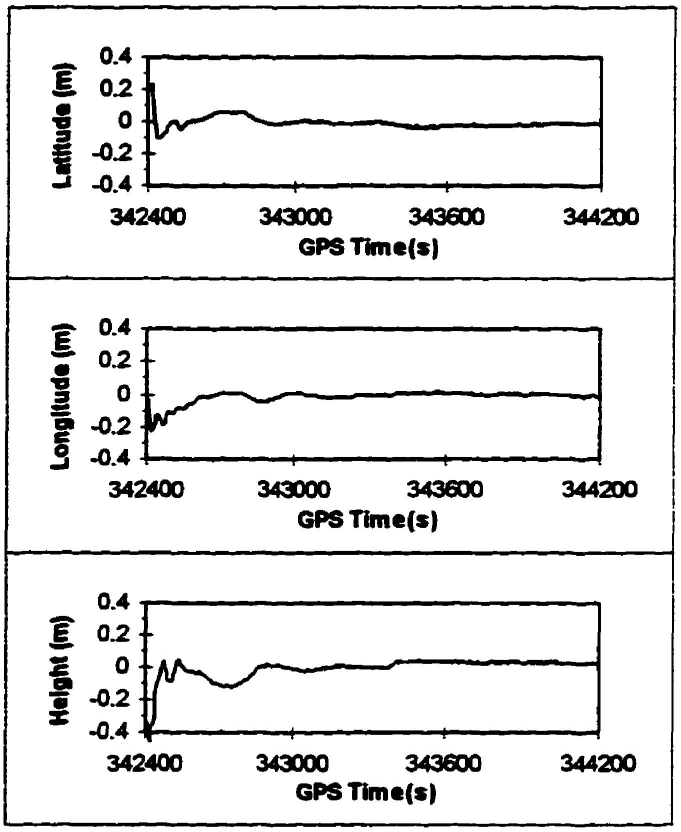

Figure 7.10: Performance of the Floating Ambiguity Solution with Quality Control (Single Bias Situation)

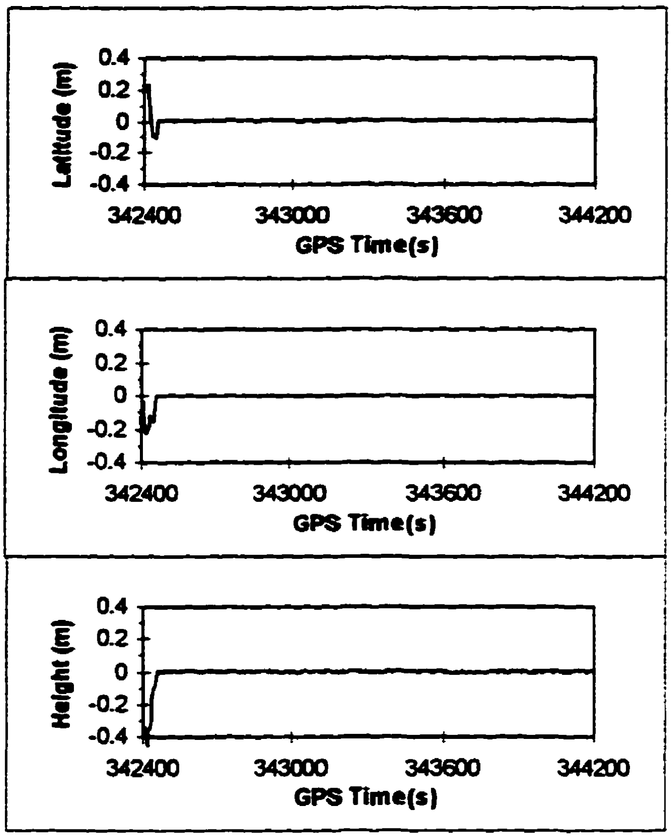

Figure 7.11 Performance of the Fixed Integer Ambiguity Solution with Quality Control (Single Bias Situation)

It can be seen from Figure 7.8 that one cycle (19 cm) bias in Satellite 15 carrier phase observations caused about 30 cm, 20 cm and 40 cm errors for the three coordinate components in the floating ambiguity solution at the beginning. The errors reduced later on because the floating ambiguity of Satellite 15 changed slowly to fit the biased carrier phase observations. As for the fixed integer ambiguity solution, the one cycle bias caused 8 cm, 7 cm and 12 cm constant errors for the three coordinate components without quality control (see Figure 7.9)

When quality control was on, the one cycle bias was detected and recovered. No error was injected into both floating ambiguity and fixed integer ambiguity solution (see Figures 7.10 and 7.11).

Another simulation was done with two biases. One cycle was added to the observations of both Satellite 15 and 2 beginning at GPS epoch 343400. The performances of both floating ambiguity and fixed integer ambiguity solution with quality control on are shown in Figures 7.12 and 7.13. It can be seen that the biases incurred position errors although quality control was on. The quality control methods applied here cannot handle multi-bias situation.

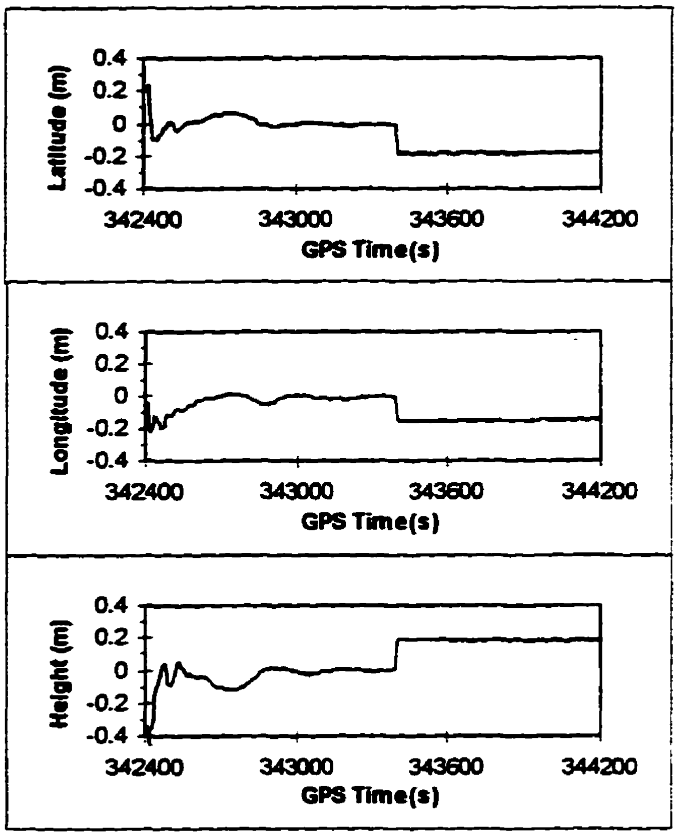

Figure 7.12: Performance of the Floating Ambiguity Solution with Quality Control (Two Biases Situation)

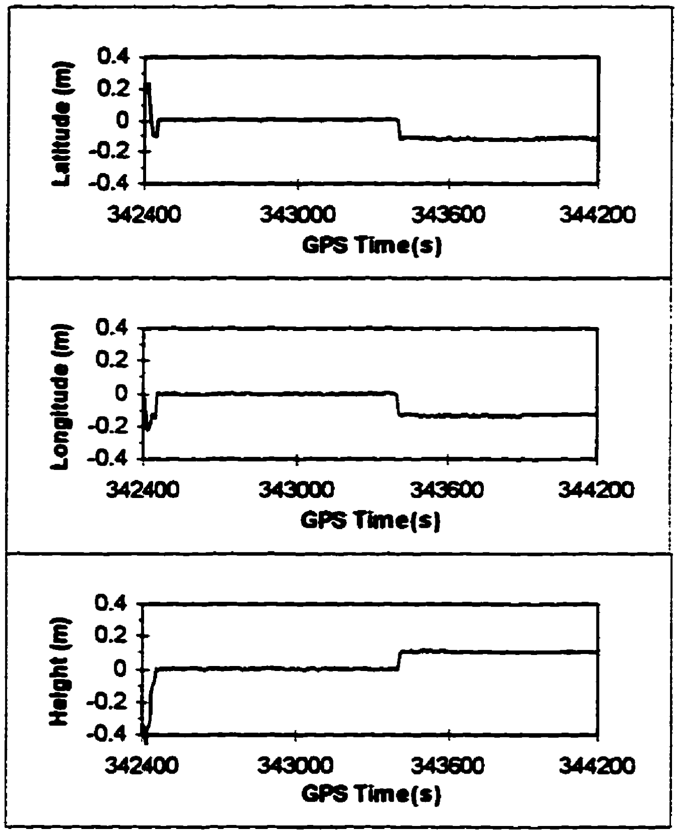

Figure 7.13 Performance of the Fixed Integer Ambiguity Solution with Quality Control (Two Biases Situation)

7.2 Kinematic Tests

The objective of the kinematic tests was to evaluate the performance of the system when the rover was in a dynamic environment. Two tests were conducted as described in the following sections.

7.2.1 Precise Farming Test

A kinematic test was performed on October 19, 1995, in conjunction with a precision farming project conducted in Southern Alberta [Lachapelle et al., 1994]. The system was used to locate 70 predefined points spaced 50 m apart. This specific test was used for soil sampling, in order to evaluate the relationship between yield and soil quality. A truck was used as the rover, with a GPS antenna and a radio antenna on the roof. Choke rings were used at both the reference station and the rover. Two NovAtel GPSCard™ receivers were used. A portable computer and a radio transceiver were placed inside the vehicle. The truck was navigated to a point, which was located by moving the antenna until position results matched the predefined coordinates. A stake was set at the point, and the truck then continued to the next point. The trajectory of the truck is shown in Figure 7.14.

The points with predefined coordinates were located by viewing the real-time position output of the system. Only the real-time floating ambiguity solution was generated in this case since the required accuracy was 0.5 m.

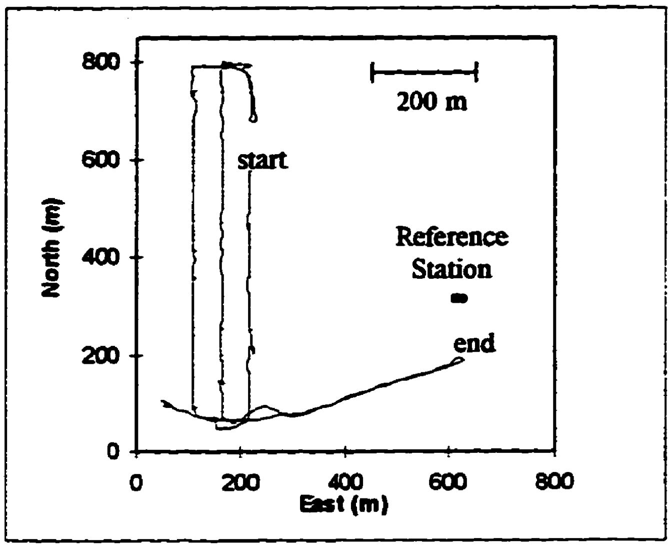

Figure 7.14: Truck Trajectory

The raw GPS data for the kinematic test was recorded, as well as the real-time results. The raw data was post-processed using FLYKIN™. The distances between reference and rover stations ranged from 50 m to 1 km. Six satellites were continuously available above a 10° cut-off angle. The PDOP values were less than 3.0 throughout the test. Integer ambiguities were fixed after 15 epochs (15 s) and the trajectory of the truck was resolved to the centimetre level accuracies. The real-time results were then compared with the high accuracy trajectory, and the differences are shown in Figure 7.15.

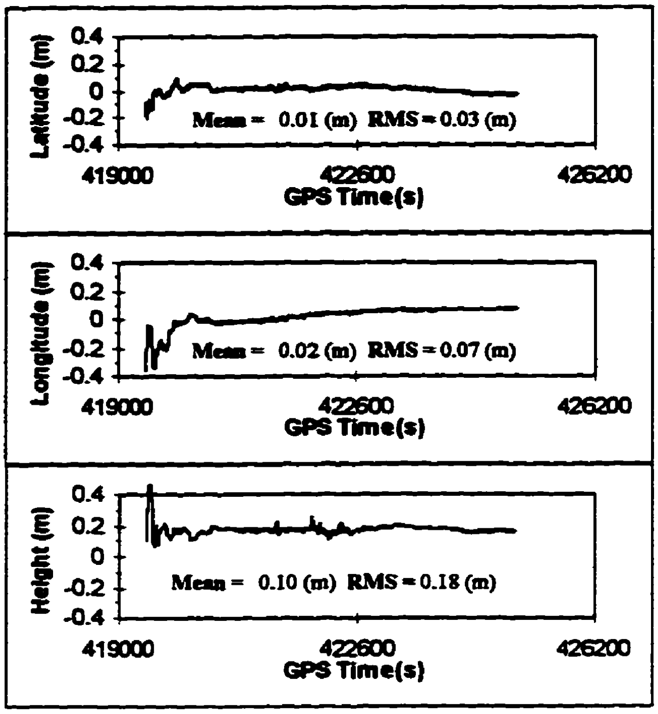

Figure 7.15: Differences Between Real-Time Results and the Post Processed High Accuracy Trajectory

RMS values of the latitude and longitude components are less than 10 cm. The RMS value of height is larger, but is still less than 20 m. This demonstrates that the real-time kinematic floating ambiguity solution has at accuracies at 20 cm level, consistent with the RT20 results [Ford and Neumann, 1994], and the 0.5 m accuracy requirement is satisfied.

7.2.2 Kinematic Surveying Test

Another kinematic test was performed on March 2, 1996, at Springbank (14 km west of Calgary), where there are three pillars whose coordinates were accurately determined to a few cm accuracy in a static GPS survey. Pillar 661-24-8 was used as the reference station, with a NovAtel GPS antenna and a choke ring placed on top of the pillar. The other two pillars were used as check points for comparison with real-time results (see Figure 7.16). The rover was a car with a NovAtel antenna, a choke ring, and radio antenna placed on the roof. Two NovAtel GPS OEM sensors were used in this test.

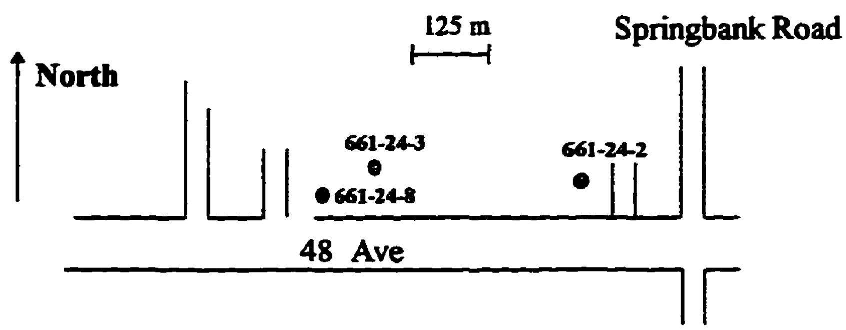

Figure 7.16: Sketch of Springbank Pillars

The first trial of the kinematic test began at the reference station (see Figure 7.17). Integer ambiguities were fixed after 105 epochs (1 Hz data rate). Seven satellites were available above a 10° cut-off angle initially, and the PDOP values were approximately 2.0 (see Figure 7.18). The distance between the reference and the rover was approximately 6 m. The rover then moved from the reference station to the check point I (661-24-3 in Figure 7.16), where the GPS antenna was placed on top of the pillar. After about one minute, the antenna was placed back on the car roof.

The second trial began at the check point II (661-24-2 in Figure 7.17). Five satellites were available above a 10° cut-off angle initialy, and satellite geometry was poor, such that PDOP values were larger than 6.0 (see Figure 7.18). After one minute, another two satellites were acquired and PDOP values decreased to less than 3.0. It took 232 epochs for the system to resolve the integer ambiguities because of the poor initial satellite geometry. The distance between reference and rover was approximately 442 m. The GPS antenna was placed on top of check point II for one minute. The antenna was then placed back on the top of the rover which moved to check point I along 48th Avenue. The antenna was placed on check point I for one minute, and the rover then moved west along 48th Avenue. back to the reference station.

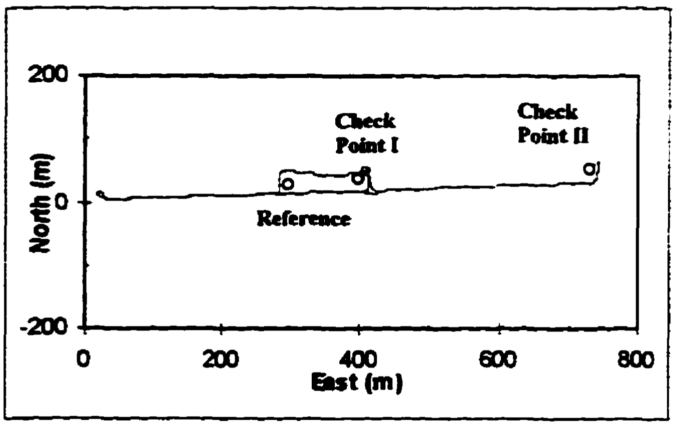

Figure 7.17: Car Trajectory

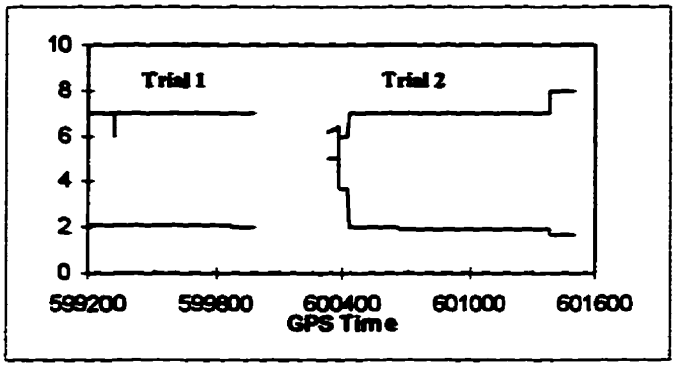

Figure 7.18: Satellite Number and PDOP (Kinematic Test, Springbank)

The real-time floating ambiguity solution was compared with the post-processed fixed integer ambiguity solution results. Differences are plotted in the Figure 7.19. Additionally, the real-time floating and fixed integer ambiguity position solutions were compared with the known coordinates of check point I and II which were obtained from a static survey. The differences are shown in Tables 7.1 and 7.2.

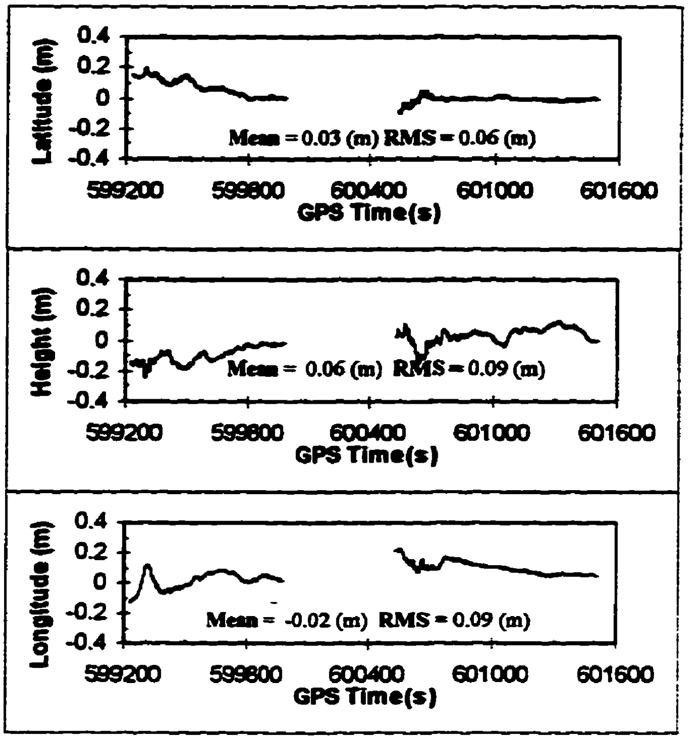

Figure 7.19: Differences Between the Real-Time Floating Ambiguity Solution and Post-Processed Fixed Integer Ambiguity Solution (Kinematic Test, Springbank)

Table 7.1: Differences Between Real-Time Floating Ambiguity Solution Results and Known Coordinates

		Latitude (m)	*Longitude* (m)	*Height* (m)
Check Point I (first trial)	**Mean**	-0.01	0.00	0.02
	RMS	0.01	0.00	0.02
Check Point I (second trial)	**Mean**	-0.01	0.10	0.04
	RMS	0.01	0.11	0.04
Check Point II	**Mean**	0.04	0.07	-0.09
	RMS	0.04	0.07	0.09

Table 7.2: Differences Between Real-Time Fixed Integer Ambiguity Solution Results and Known Coordinates

		Latitude (m)	*Longitude* (m)	*Height* (m)
Check Point I (first trial)	**Mean**	-0.01	0.00	0.04
	RMS	0.01	0.00	0.04
Check Point I (second trial)	**Mean**	-0.02	0.00	0.04
	RMS	0.02	0.00	0.04
Check Point II	**Mean**	0.00	0.00	0.05
	RMS	0.00	0.00	0.05

In Figure 7.19, the RMS values of the floating ambiguity solutions are 0.06 m, 0.09 m and 0.09 m for the latitude, longitude and height coordinate components respectively. Comparing with coordinates of check points, the largest RMS value for the floating ambiguity solution is 0.11 m (see Table 7.1), while the largest RMS value for the fixed integer ambiguity solution is 0.05 m (see Table 7.2), demonstrating that centimetre-level accuracies were achieved in this test. It is also shown from Tables 7.1 and 7.2 that the largest differences occur in the height component, verifying that height accuracies are worse than horizontal acuracies in GPS positioning.

CHAPTER EIGHT

CONCLUSIONS AND RECOMMENDATIONS

8.1 Conclusions

The objective of this research was to develop a RTK GPS system for high accuracy positioning in real-time. The design, performance and results of the RTK GPS system are presented in this thesis.

The system hardware was developed by integrating of two NovAtel GPSCard™ receivers (or two NovAtel OEM GPS sensors), two Hopper™ radio transceivers, two NovAtel geodetic GPS antennae (with choke-rings) and two portable computers.

The system software was based on FLYKIN™ and a number of data communication routines available in the Department of Geomatics Engineering at The University of Calgary. The following system software components were developed by the author: a) data communication between the laptop computers and the GPS receivers; b) real-time data logging and preprocessing; c) data communication between the laptop computers and the radio transceivers; d) generating the carrier phase and pseudorange corrections; e) encoding the raw observations and their corrections into RTCM types 18-21 formats and The U of C formats; f) processing carrier phase and pseudorange corrections as well as raw Doppler data; and g) floating ambiguity solution and statistical testing based on the innovation sequence. The RTK GPS system has the following features:

a) The system output rate is 1 Hz;

b) The system has the option of floating or fixed integer ambiguity solutions. Decimetre or centimetre level accuracy can be achieved, based on the type of solution chosen;

c) The system can perform positioning by transmitting and receiving raw observations (carrier phase, pseudorange and Doppler observations) or the carrier phase and pseudorange corrections. The system can also generate and accept RTCM types 18-21 messages; and

d) The system has quality control of both floating ambiguity and fixed integer ambiguity solutions, in order to ensure that output results are as reliable as possible.

Various tests were conducted to evaluate the system performance. For the short baseline, short time period, static test, RMS values for the floating (fixed integer) ambiguity solution are 6 cm (3 cm) or better for each of the three position components. For the short baseline, long time period, static test, RMS values for the floating (fixed integer) ambiguity position solution are 7 cm (1 cm) or better for each position coordinate. The long, 14 hour, test demonstrates that the system can operate reliably over a long period of time. The quality control simulation results show that this system can detect the bias and recover successfully when a bias happens.

Kinematic test results, for the precise farming project, demonstrated that the real-time floating ambiguity solution is reliable for decimeter level accuracy, after the initial filter convergence (which typically takes 5 minutes). To achieve centimetre level accuracy, the system must implement a fixed integer ambiguity solution, which is computed using the FASF algorithm.

The kinematic surveying test in Springbank demonstrated that the system can achieve centimetre level accuracy, as determined from a comparison of the real-time fixed integer ambiguity position solution with the known coordinates of two check points. The largest RMS value was 5 cm, in the height component.

Test results show that the carrier phase and pseudorange corrections are suitable for a real-time GPS system. Using these corrections are more effective than using raw GPS data, since fewer bits are required for transmission (if using The U of C format). Additionally, the number of computations required at the rover is reduced when corrections, rather than raw measurements, are transmitted.

8.2 Recommendations

A pair of Hopper™ transceivers, with 1 W transmit power, were used in this RTK GPS system. Although the manual accompanying these transceivers lists a transmission range of 30 km, the transmission range was limited to 1 km in tests conducted for the purposes of this research. To achieve long distance real-time positioning, another pair of more powerful radio transceivers should be used.

Test results show that the integer ambiguities can be fixed reliably by this system when NovAtel single frequency receivers are used. In general, however, the remaining error sources for double difference observations are spatially-correlated, and it is difficult to fix the integer ambiguities reliably using single frequency receivers when the reference-rover separation is over about 10 km (see Chapter 2). Dual frequency receivers should be used to achieve high accuracy in the case of a long reference-rover separation.

Although this system was designed for NovAtel GPS receivers, the system can be adapted for other types of receivers, through minor modifications of the software.

REFERENCES

Abousalem, M.A. (1996). Development and Analysis of Wide Area Differential GPS Algorithm. Ph. D Dissertation of Department of Geomatics Engineering, No. 20083, The University of Calgary.

Aparicio, M., P. Brodie, and J. Rajan (1994). Communication Satellite Augmented GPS Payload Architecture. Proceedings of ION GPS-94, Salt Lake City, Utah, Sept. 20-23, The Institute of Navigation, pp. 1007-1016.

Baarda, W. (1968). A Testing Procedure for Use in Geodetic Networks. Netherlands Geodetic Commission, Publications on Geodesy, New Series 2, No.5 Delft.

Blomenhofer, H., and G. W. Hein (1994). Development of A Real-Time DGPS System in the Centimeter Range. Proceedings of IEEE Position Location and Navigation Symposia, Las Vegas, Nevada, April 11-15, pp. 532-539.

Cannon, M. E. (1991). Airborne GPS/INS with an Application to Aerotriangulation. Report No. 20040, Department of Geomatics Engineering, The University of Calgary.

Cannon, M. E. (1989). High Accuracy GPS Semi-kinematic Positioning: Modeling and Results. Proceedings of The Institute of Navigation 2nd International Technical Meeting on GPS, Colorado Springs, CO, Sept. 27-29, pp. 405-418.

Chen, D., and G. Lachapelle (1994). A Comparison of the FASF and Least-Squares Search Algorithms for Ambiguity Resolution On The Fly. Proceedings of the International Symposium on Kinematic Systems in Geodesy, Geomatics, and Navigation (KIS-94), Banff, Canada, Aug. 30 - Sept. 2, pp. 241-253.

Dedes, G. (1994). Performance and Commercialization Efforts of the Centre for Mapping Real-Time Cm-Level GPS Positioning System. Proceedings of the International Symposium on Kinematic Systems in Geodesy, Geomatics, and Navigation (KIS-94), Banff, Canada, Aug. 30 - Sept. 2, pp. 279-285.

Fenton, P. C., B. Falkenberg, T. Ford, K. Ng and A. J. VanDierendonck (1991). NovAtel's GPS receiver - The High Performance OEM Sensor of the Future. Proceedings of ION GPS-91, Albuquerque, NM, Sept. 11-13, The Institute of Navigation.

Ford, T., and J. Neumann (1994). NovAtel's RT20 - A Real Time Float Ambiguity Positioning System. Proceedings of ION GPS-94, Salt Lake City, Utah, Sept. 20-23, The Institute of Navigation, pp. 1067-1076.

Frei, E. and G. Beutler (1990). Rapid Static Positioning Based on the Fast Ambiguity Resolution Approach: The Alternative to Kinematic Positioning. Proceedings of Second International Symposium on Precise Positioning with GPS, Canadian Institute of Geomatics, Ottawa.

Frodge, S., V. Labrecque, and R. Barker. (1995). Performance of the Real-Time On-The-Fly GPS Positioning System on Board a Dredge. Proceedings of National Technical Meeting, Anaheim, CA, Jan. 18-20, The Institute of Navigation, pp. 505-512.

Gefsrud, R., X. Qin and W. Martin (1995). Real-Time GPS Land Surveying. Proceedings of National Technical Meeting, Anaheim, CA, Jan. 18-20, The Institute of Navigation, pp. 287-292.

Gehue, H. L. (1994). GPS Integrated Systems for Precision Farming. UCGE Report No. 20072, Department of Geomatics Engineering, The University of Calgary.

Gelb, (1974). Applied Optimal Estimation. The M.I.T. Press, Cambridge, MA.

Griffioen, P., T. Allison and S. Dreier (1993). Real Time Kinematic: The Next Surveying Tool. Proceedings of 1993 National Technical Meeting of the Institute of Navigation, San Francisco, CA.

Halsall, F. (1985). Introduction to Data Communication And Computer Networks. Addison-Wesley Publishing Company, Inc., Great Britain.

Hatch, R. (1991). Instantaneous Ambiguity Resolution. Proceedings of International Association of Geodesy Symposia 107 on Kinematic Systems in Geodesy, Surveying and Remote Sensing, Springer Verlag, New York, pp. 299-308.

Hofmann-Wellenhof, B., H. Lichtenegger, and J. Collins (1994). Global Positioning System. Third, Revised Edition, Springer-Verlag Wien, Austria.

Hopper™ operation manual (1994). WiLan Ltd., Calgary, Canada.

ICD-GPS-200 (1991). Interface Control Document. U.S. Coast Guard.

Kelly, J. T. (1992). Development of a Pseudo Real-Time Kinematic Survey System (KISS). Proceedings of GPS-92, Sept. 16-18, Albuquerque, The Institute of Navigation, pp. 1015-1023.

Krakiwsky, E. J. (1990). The Method of Least Squares: A Synthesis of Advances. Lecture Note of Department of Geomatics Engineering, The University of Calgary.

Lachapelle, G. (1995). GPS Theory and Applications. Lecture Notes for ENGO 625, Department of Geomatics Engineering, The University of Calgary.

Lachapelle, G., M. E. Cannon, H. Gehue, T. W. Goddard, and D. C. Penney (1994). GPS System Integration and Field Approaches in Precision Farming. Journal of the Institute of Navigation, Vol. 41, No. 3, pp. 323-335.

Lan, H., and M. E. Cannon. Development of a Real-Time Kinematic GPS System: Design, Performance and Results. Proceedings of 1996 National Technical Meeting of the Institute of Navigation, Santa Monica, CA, Jan. 22-24, 1996.

Landau, H., and H. J. Euler (1992). On-the-fly Ambiguity Resolution for Precise Differential Positioning. Proceedings of GPS-92, Albuquerque, New Mexico, Sept. 16-18, The Institute of Navigation, pp. 607-613.

Lu, G. (1995). Development of a GPS Multi-Antenna System for Attitude Determination. Ph. D. Dissertation No. 20073, Department of Geomatics Engineering, The University of Calgary.

Lu, G. (1991). Quality Control for Differential Kinematic GPS Positioning. M. Sc. Thesis No.20042, Department of Geomatics Engineering, The University of Calgary.

Lu, G. and G. Lachapelle (1990). Reliability Analysis for Kinematic GPS Positioning and Velocity Estimation. Proceedings of IAG International Symposium 107 on Kinematic Systems in Geodesy, Surveying and Remote Sensing, Springer Verlag, New York, 1990.

Lu, G. and M. E. Cannon (1994), FLYKIN™ Operation Manual. Department of Geomatics Engineering, The University of Calgary.

Mader, G. L. (1990). Ambiguity Function Technique for GPS Phase Initialization and Kinematic Solution. Proceedings of Second International Symposium on Precise Positioning with GPS, Canadian Institute of Geomatics, Ottawa.

Mathes, A., and M. Gianniou (1994). Real-Time Rapid-Static and Kinematic Survey at the Centimeter Level and Below. Proceedings of ION GPS-94, Salt Lake City, Utah, Sept. 20-23, The Institute of Navigation, pp. 105-113.

McCall, T. (1994). The Development of a Modular DGPS System. Proceedings of ION GPS-94, Salt Lake City, Utah, Sept. 20-23, The Institute of Navigation, pp. 1299-1307.

McLellan, J. F., M. A. Abousalem, E. Whatley and P. Galyean. (1994). ACC-Q-POINT FM Subcarrier WADGPS. Proceedings of ION GPS-94, Salt Lake City, Utah, Sept. 20-23, The Institute of Navigation, pp. 1017-1024.

Neumann, J. B., A. Manz, T. J. Ford, and O. Mulyk (1996). Test Results from a New 2 cm Real Time Kinematic GPS Positioning System. Proceedings of ION GPS-96, Kansas City, Sept. 17-20, The Institute of Navigation, pp. 873-882.

Proakis, J. G. (1989). Digital Communications. Second Edition, McGraw-Hill Series in Electrical Engineering.

Remondi, B. W. (1991). Kinematic GPS Results Without Static Initialization. Proceedings of the Institute of Navigation 47th Annual Meeting, Washington, D. C. pp. 87-111.

Remondi, B. W. (1988). Kinematic and Pseudo-Kinematic GPS. Proceedings of the Institute of Navigation 1st International Technical Meeting on GPS, Colorado Springs, CO.

Remondi, B. W. (1986). Performing Centimeter Accuracy Relative Surveys in Seconds Using GPS Carrier Phase: Initial Result. Navigation, Vol. 32, No.4, pp. 194-208.

Remondi, B. W. (1985). Performing Centimeter Accuracy Relative Surveys in Seconds Using GPS Carrier Phase. Proceedings of First International Symposium on Precise Positioning with GPS, Rockville, Maryland, April, pp. 789-797.

Robbins, J. (1994). Global Corrections for GPS. Proceedings of ION GPS-94, Salt Lake City, Utah, Sept. 20-23, The Institute of Navigation, pp. 1025-1033.

RTCM (1994). Recommended Standards for Differential Navstar GPS Service (version 2.1). RTCM SC-104. Washington, D. C.

Seeber, G. (1993). Satellite Geodesy. Walter de Gruter, Berlin.

Schwarz, K. P., Z. Liu, and J. Q. Zhang. (1994). Testing a Radio Link System for Real-Time DGPS Velocity Determination. Proceedings of ION GPS-94, Salt Lake City, Utah, Sept. 20-23, The Institute of Navigation, pp. 1491-1498.

Sushko, M. S. K. (1994). Characteristics of a Combined DGPS Code/Carrier-Phase Correction Broadcast Channel. Proceedings of the International Symposium on Kinematic Systems in Geodesy, Geomatics, and Navigation (KIS-94), Banff, Canada, Aug. 30 - Sept. 2, pp. 299-311.

Space News (1994). USA, April 1-7.

Taveira-Blomenhofer, E., and G. W. Hein (1993). Investigation on Phase Corrections for High-Precision DGPS Navigation. Proceedings of ION GPS-93, Salt Lake City, Utah, Sept. 22-24, The Institute of Navigation, pp. 1461-1467.

Teunissen, P. J. G. (1990). Quality Control in Integrated Navigation Systems. Proceedings of IEEE PLANS'90, Las Vegas, USA.

Teunissen, P. J. G. and M. A. Salzmann (1989). A Recursive Slippage Test for Use in State-Space Filtering. Manuscripta Geodaetica, Vol. 14, pp. 383-390.

Teunissen, P.J.G. and C.C.J.M. Tiberius (1994). Integer Least-Squares Estimation of the GPS Phase Ambiguities. Proceedings of the International Symposium on Kinematic Systems in Geodesy, Geomatics, and Navigation (KIS-94), Banff, Canada, Aug. 30 - Sept. 2, pp. 221-231.

Walsh, D., V. Ashkenazi, and G. Ffoulkes-Jones (1995). Performance of OTF Ambiguity Resolution Search Algorithms for Real Time Positioning Under Varying Conditions. Proceedings of National Technical Meeting, Anaheim, CA, Jan 18-20, The Institute of Navigation, 1995, pp. 313-321.

Wei, M., D. Lapucha and H. Martell (1990). Fault Detection and Estimation in Dynamic Systems. Proceedings of IAG International Symposium 107 on Kinematic Systems in Geodesy, Surveying and Remote Sensing, Springer Verlag, New York.

Wells, D., N. Beck, D. Delikaragoglou, A. Kleusberg, E. J. Krakiwsky, G. Lachapelle, R. B. Langley, M. Nakiboglu, K. P. Schwarz, J. M. Tranquilla, and P. Vanicek (1986). Guide to GPS Positioning. Canadian GPS Associaties, Fredericton, New Brunswick, Canada.

Van Dierendonck, A. J., and P. Enge (1994). The Wide Area Augmentation System (WAAS) Signal Specification. Proceedings of ION GPS-94, Salt Lake City, Utah, Sept. 20-23, The Institute of Navigation, pp. 985-994.

APPENDIX

KALMAN FILTER EQUATIONS

The dynamics of a kinematic system can be described by the state model described in equation (3.1). Solving the differential equation (3.1), the system model of a discrete Kalman filter is derived [Gelb, 1974]:

$$\mathbf{x}_{k+1} = \Phi_{k+1,k}\mathbf{x}_k + \mathbf{w}_k , \tag{A.1}$$

where subscripts k, k+1 are time epochs,

$\Phi = e^{F\Delta t} \approx \mathbf{I} + \mathbf{F}\Delta t$ is the transition matrix $(m \times m)$,

Δt is the time interval between epoch k+1 and epoch k,

$\mathbf{w}_k$ is the process noise, assumed to have a zero-mean Gaussian distribution

$\mathbf{w}_k \sim N(0, C_k^w)$,

$\mathbf{C}_k^w = \int_0^{\Delta t} \Phi(\tau)\mathbf{Q}(\tau)\Phi^T(\tau)d\tau \approx \mathbf{Q}\Delta t$ is the variance-covariance matrix of the process noise $(m \times m)$,

τ refers to correlation time,

and $\mathbf{Q}$ is the spectral density matrix $(m \times m)$.

The Kalman prediction equations can be derived from equation (A.1) as

$$\mathbf{x}_{k+1}(-) = \mathbf{\Phi}_{k+1,k}\mathbf{x}_k(+), \tag{A.2}$$

and $$\mathbf{C}^x_{k+1}(-) = \mathbf{\Phi}_{k+1,k}\mathbf{C}^x_k(+)\mathbf{\Phi}^T_{k+1,k} + \mathbf{C}^w_k, \tag{A.3}$$

where (-) denotes predicted quantities, (+) denotes updated quantities, and $\mathbf{C}^x$ is the $(m \times m)$ variance-covariance matrix of the state vector.

The observations at epoch k+1 are related to the state vector as follows:

$$\mathbf{z}_{k+1} = \mathbf{H}_{k+1}\mathbf{x}_{k+1} + \varepsilon, \tag{A.4}$$

where $\mathbf{z}_{k+1}$ is the observation vector $(l \times 1)$, l being the number of observations,

$\mathbf{H}_{k+1}$ is the design matrix $(l \times m)$,

ε is the measurement noise vector $(l \times 1)$ assumed to have a zero-mean Gaussian distribution $\varepsilon \sim N(0, \mathbf{C}^\varepsilon)$,

$\mathbf{C}^\varepsilon$ is the variance-covariance matrix of ε,

and m is the number of unknown parameters.

Kalman filter update equations are used to estimate the state vector

$$\mathbf{x}_{k+1}(+) = \mathbf{x}_{k+1}(-) + \mathbf{K}\left[\mathbf{z}_{k+1} - \mathbf{H}_{k+1}\,\mathbf{x}_{k+1}(-)\right], \tag{A.5}$$

$$\mathbf{C}^{x}_{k+1}(+) = \left[\mathbf{I} - \mathbf{K}\mathbf{H}_{k+1}\right]\mathbf{C}^{x}_{k+1}(-), \tag{A.6}$$

with

$$\mathbf{K} = \mathbf{C}^{x}_{k+1}(-)\mathbf{H}^{T}_{k+1}\left[\mathbf{H}_{k+1}\mathbf{C}^{x}_{k+1}(-)\mathbf{H}^{T}_{k+1} + \mathbf{C}^{\varepsilon}\right]^{-1}, \tag{A.7}$$

where $\mathbf{x}_{k+1}(+)$ is the $(m \times 1)$ updated state vector,

$\mathbf{C}^{x}_{k+1}(+)$ is the $(m \times m)$ variance-covariance matrix of $\mathbf{x}_{k+1}(+)$,

$\mathbf{C}^{\varepsilon}$ is the $(l \times l)$ variance-covariance matrix of measurement noise vector ε,

$\mathbf{K}$ is the $(m \times l)$ Kalman filter gain matrix.

A simpler form for the gain matrix can be written as [Gelb, 1974]

$$\mathbf{K} = \mathbf{C}^{x}_{k+1}(+)\mathbf{H}^{T}_{k+1}\mathbf{C}^{\varepsilon^{-1}} = \left[\mathbf{C}^{x}_{k+1}(-)^{-1} + \mathbf{H}^{T}_{k+1}\mathbf{C}^{\varepsilon^{-1}}\mathbf{H}_{k+1}\right]^{-1}\mathbf{H}^{T}_{k+1}\mathbf{C}^{\varepsilon^{-1}}. \tag{A.8}$$